

Superconductivity in LaH₁₀: a new twist of the story

Ivan A. Kruglov,^{1,2,*} Dmitrii V. Semenok,^{1,3} Radosław Szczęśniak,^{4,5} M. Mahdi Davari Esfahani,⁶ Alexander G. Kvashnin^{3,1} and Artem R. Oganov^{3,2,7}

¹ Moscow Institute of Physics and Technology, 141700, 9 Institutsky lane, Dolgoprudny, Russian Federation

² Dukhov Research Institute of Automatics (VNIIA), Moscow 127055, Russian Federation

³ Skolkovo Institute of Science and Technology, Skolkovo Innovation Center 143026, 3 Nobel Street, Moscow, Russian Federation

⁴ Institute of Physics, Jan Dlugosz University in Czestochowa, Ave. Armii Krajowej 13/15, 42-200 Czestochowa, Poland

⁵ Institute of Physics, Częstochowa University of Technology, Ave. Armii Krajowej 19, 42-200 Czestochowa, Poland

⁶ Department of Geosciences and Center for Materials by Design, Institute for Advanced Computational Science, State University of New York, Stony Brook, NY 11794-2100, USA

⁷ International Center for Materials Discovery, Northwestern Polytechnical University, Xi'an, 710072, China

Corresponding Author

*Ivan Kruglov, E-mail: ivan.kruglov@phystech.edu

ABSTRACT. We study the high-pressure chemistry of the La-H system and superconducting properties of the predicted lanthanum hydrides. A $Fm\bar{3}m$ -LaH₁₀+3H₂→ $P6/mmm$ -LaH₁₆ reaction leading to a new superconducting superhydride LaH₁₆ with critical temperature (T_C) of 219-243 K, upper critical field $H_C(0)$ ~50 T and superconducting gap up to 53 meV was found at pressures over 200 GPa. Besides LaH₁₆, in the framework of Bardeen-Cooper-Schrieffer theory we analyzed in details superconducting properties of LaH₁₀ recently studied by Drozdov et al. [1] and Somayazulu et al. [2], where T_C was estimated to be 215-245 K. For better agreement between theory and experiment in LaH₁₀ a Coulomb pseudopotential μ^* should be more than 0.2-0.28. Upper critical field in LaH₁₀ was evaluated as 76-100 T, isotopic coefficient β was calculated to be 0.41-0.46 and T_C (LaD₁₀) is 156-184 K. The difference between experimental data may be alternatively explained by the existence of $Fm\bar{3}m$ and $R\bar{3}m$ allotrope modifications of LaH₁₀ with far different superconducting temperatures.

Introduction

Recently, superhydrides of various elements attracted enormous attention: under high pressure they exhibit high-temperature superconductivity. Following Bardeen-Cooper-Schrieffer (BCS) theory, metallic hydrogen is expected to be a high- T_C superconductor [3,4], yet the pressures needed for its formations are too high [5]. One way to lower the pressure is to study metallic hydrides, since hydrogen atoms there are initially “chemically precompressed” [6]. There are many theoretical predictions for potential high-temperature superconductors (HTSC) in such systems: Ca-H [7], Y-H [8], H-S [9], Th-H [10], Ac-H [11], La-H [12].

The first experimental work, which supported these ideas, confirmed superconductivity in H₃S with T_C = 203 K at 155 GPa [13] (while calculated value was 191-204 K at 200 GPa [9]). The agreement between the measured and calculated values reassured scientific community and generated a wave of theoretical studies related to the study of superconductivity in hydrides [11,12,14-28]. Recent theoretical work on the investigation of La-H and Y-H systems [27] under pressure showed that LaH₁₀ and YH₁₀ at 300 GPa may display superconductivity at near-room temperatures (286-326 K). Experimental observation of the sharp reduction of resistivity in the LaH_{10+x} samples was the first evidence of possible

superconductivity [1,2]. However, T_C values measured by A. Drozdov et al. [1] and Somayazulu et al. [2] were different, 215 and 260 K, respectively. This may be explained by the existence of different phases of LaH_{10} . According to Geballe et al. [17], $R\bar{3}m$ - LaH_{10} was stable at 160–170 GPa (where A. Drozdov et al. [1] made measurements), while $Fm\bar{3}m$ - LaH_{10} – at higher pressures [17] (where Somayazulu et al. [2] performed experiments). Despite of the fact that superconductivity in LaH_{10} was detected only by resistive method in the absence of an external magnetic field [1,2], these T_C values can be used to determine other parameters of the superconducting state using the Eliashberg theory [29,30].

In order to clarify the results obtained in the recent articles [12,17,31,32], we performed variable-composition search using evolutionary algorithm USPEX [33–35] in La-H system. We found a new stable superhydride $P6/mmm$ - LaH_{16} . The superconducting properties of $P6/mmm$ - LaH_{16} and $Fm\bar{3}m$ - LaH_{10} phases were analyzed in more details.

Computational details

Evolutionary algorithm USPEX [33–35] is a powerful tool for predicting thermodynamically stable compounds of given elements at a given pressure. To predict thermodynamically stable phases in the La-H system we performed a variable-composition crystal structure searches at pressures of 50 and 150 GPa. The first generation of 100 structures was created using random symmetric generator, while all subsequent generations contained 20% random structures, and 80% created using heredity, softmutation and transmutation operators. Here, evolutionary searches were combined with structure relaxations using density functional theory (DFT) [36,37] within the generalized gradient approximation (Perdew-Burke-Ernzerhof functional) [38], and the projector-augmented wave method [39,40] as implemented in the VASP package [41–43]. Plane wave kinetic energy cutoff was set to 500 eV and the Brillouin zone was samples by Γ -centered k -points meshes with resolution $2\pi \times 0.05 \text{ \AA}^{-1}$.

In order to establish stability fields of the predicted phases, we recalculated their enthalpies with increased precision at various pressures with a smaller pressure increment (from 5 to 10 GPa), recalculating the thermodynamic convex hull (Maxwell construction) at each pressure. Phases that are on the convex hull are the ones stable at given pressure. Stable structures of elemental La and H were taken from USPEX calculations and from Refs. [44] and [45], respectively.

Calculations of critical temperature and electron-phonon coupling (EPC) parameters were carried out using Quantum ESPRESSO package [46] within density-functional perturbation theory [47], employing plane-wave pseudopotential method and Perdew-Burke-Ernzerhof exchange-correlation functional [38]. Convergence tests showed that 90 Ry is a suitable kinetic energy cutoff for the plane wave basis set. Electronic band structures along with phonon densities of states of $P6/mmm$ - LaH_{16} and $Fm\bar{3}m$ - LaH_{10} were calculated using both VASP (finite displacement method using PHONOPY [48,49]) and QE (density-functional perturbation theory [47]), which demonstrated good consistency.

In our calculations of the EPC parameter λ , the first Brillouin zone was sampled using $2 \times 2 \times 2$ and $4 \times 4 \times 4$ q -points mesh, and a denser $16 \times 16 \times 16$ k -points mesh (with Gaussian smearing and $\sigma = 0.02$ Ry, which approximates the zero-width limits in the calculation of λ).

Critical temperature was calculated from the Eliashberg equation [29] which is based on the Fröhlich Hamiltonian $\hat{H} = \hat{H}_e + \hat{H}_{ph} + \sum_{k,q,j} g_{k+q,k}^{q,j} \hat{c}_{k+q}^+ \hat{c}_k (\hat{b}_{-q,j}^+ + \hat{b}_{q,j})$, where c^+ , b^+ are creation operators of electrons and phonons, respectively. Matrix element of electron-phonon interaction $g_{k+q,k}^{q,j}$ calculated within the harmonic approximation in Quantum ESPRESSO can be defined as

$$g_{k+q,k}^{q,j} = \sqrt{\frac{\hbar}{2M\omega_{q,j}}} \int \psi_k^*(r) \cdot \left\{ \frac{dV_{scf}}{du_q} \cdot \frac{\vec{u}_q}{|\vec{u}_q|} \right\} \cdot \psi_{k+q}(r) d^3r, \text{ where } u_q \text{ is the displacement of an atom with mass } M \text{ in the phonon mode } q,j. \text{ Within the framework of Gor'kov and Migdal approach [30,50]}$$

the correction to the electron Green's function $\Sigma(\vec{k}, \omega) = G_0^{-1}(\vec{k}, \omega) - G^{-1}(\vec{k}, \omega)$ caused by interaction can be calculated by taking into account only the first terms of the expansion of electron-phonon interaction in series of (ω_{\log}/E_F) . This leads to integral Eliashberg equations [29]. These equations can be solved by iterative self-consistent method for the real part of the order parameter $\Delta(T, \omega)$ (superconducting gap) and the mass renormalization function $Z(T, \omega)$ [51] (see Supporting Information).

The superconducting transition temperature T_C was also estimated by using two equations: Allen-Dynes and modified McMillan equation [52]. The Allen-Dynes equation for calculating T_C has the following form [52]:

$$T_C = \omega_{\log} \frac{f_1 f_2}{1.2} \exp \left(\frac{-1.04(1 + \lambda)}{\lambda - \mu^* - 0.62\lambda\mu^*} \right) \quad (1)$$

with

$$f_1 f_2 = \sqrt[3]{1 + \left(\frac{\lambda}{2.46(1 + 3.8\mu^*)} \right)^{\frac{3}{2}}} \cdot \left(1 - \frac{\lambda^2(1 - \omega_2/\omega_{\log})}{\lambda^2 + 3.312(1 + 6.3\mu^*)^2} \right), \quad (2)$$

while the modified McMillan equation has similar form but with $f_1 f_2 = 1$. The EPC parameter λ , logarithmic average frequency ω_{\log} and mean square frequency ω_2 were calculated as:

$$\lambda = \int_0^{\omega_{\max}} \frac{2 \cdot \alpha^2 F(\omega)}{\omega} d\omega \quad (3)$$

and

$$\omega_{\log} = \exp \left(\frac{2}{\lambda} \int_0^{\omega_{\max}} \frac{d\omega}{\omega} \alpha^2 F(\omega) \ln(\omega) \right), \quad \omega_2 = \sqrt{\frac{1}{\lambda} \int_0^{\omega_{\max}} \left[\frac{2\alpha^2 F(\omega)}{\omega} \right] \omega^2 d\omega}, \quad (4)$$

where μ^* is the Coulomb pseudopotential.

Crystal structures of predicted phases were generated using VESTA software [53].

Results and Discussion

1. Phases stability

We performed variable-composition evolutionary crystal structure and compound searches at 50 and 150 GPa in order to predict stable phases in the La-H system. Thermodynamic convex hull diagrams are shown in Fig. 1. If the phase appeared on the convex hull line, then we considered it to be stable at given pressure. Thus, at 50 GPa we found $Fm\bar{3}m$ -LaH, $Pnma$ -LaH₃ and $Cmc2_1$ -LaH₇ to be stable (see Fig. 1a). At 150 GPa chemistry of lanthanum hydrides becomes much richer: $P6/mmm$ -LaH₂, $Cmcm$ -LaH₃, $Cmmm$ -La₃H₁₀, $P\bar{1}$ -LaH₅, $Fm\bar{3}m$ -LaH₁₀ and $P6/mmm$ -LaH₁₆ become stable, see Fig. 1b.

Composition 1:1 is common for various hydrides (e.g., U-H [54], Fe-H [20] and many others [55]). $Fm\bar{3}m$ -LaH has a rocksalt-type structure, with La-H distance of 2.26 Å at 50 GPa. In $Pnma$ -LaH₃ structure hydrogen atoms are aligned along one direction, while the distances between them are too long for making a bond – 2.28 Å at 50 GPa. La-H bond distances vary between 2.14 and 2.29 Å. Coordination number of La in $Pnma$ -LaH₃ equals to 10. In $Cmc2_1$ -LaH₇ the bond length between La and H varies from 2.18 to 2.30 Å, while the coordination number is higher than in $Pnma$ -LaH₃ and equals to 13. Minimal H-H bond in this structure equals to 0.81 Å at 50 GPa, which is close to the H-H bond length in molecular hydrogen.

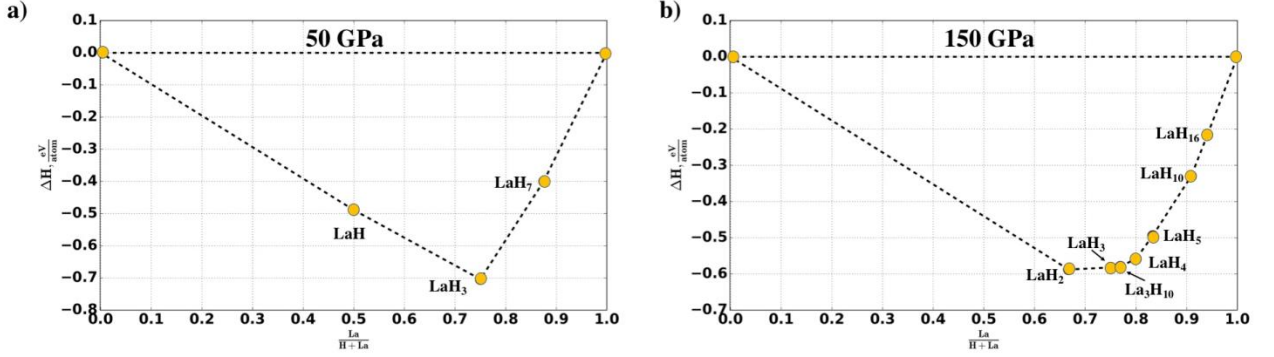


Fig. 1. Convex hull diagrams for La-H system at a) 50 and b) 150 GPa.

At higher pressure of 150 GPa we obtained results similar to the ones at Ref. [27]. Yet, besides previously known phases, we also found *Cmmm*-La₃H₁₀, which can be found only using variable-composition search as implemented in the USPEX code. This phase is structurally similar to *Cmcm*-LaH₃, but with lattice parameter *c* 3 times higher compared to LaH₃. We also found *Fm* $\bar{3}$ *m*-LaH₁₀ to be more stable than *R* $\bar{3}$ *m*-LaH₁₀ at 150 GPa. The phase transition *R* $\bar{3}$ *m* \rightarrow *Fm* $\bar{3}$ *m* occurs at 128 GPa, see Fig. S20 in Supporting Information. Including zero-point energy shifts this transition pressure to 150 GPa. Obtained result agrees with experimental data [17], where *R* $\bar{3}$ *m* undergoes a phase transition into *Fm* $\bar{3}$ *m*-LaH₁₀ at 160 GPa. Crystal structures of both LaH₁₀ phases are shown on Fig. 2a,b. For discussions of these crystal structures, see Refs. [12,17].

The most intriguing part here is that besides hydrogen-rich LaH₁₀ phases we also found *P6*/*mmm*-LaH₁₆ to be stable at 150 GPa (see Fig. 1b). The LaH₁₆ phase has the same composition, but different crystal structure compared to AcH₁₆ [28]. LaH₁₆ has *P6*/*mmm* space group, while for AcH₁₆ it is *P* $\bar{6}$ *m*2. Lanthanum atoms form an hcp sublattice where hydrogen atoms lie in the interstitials between lanthanum atoms (see Fig. 2c), forming cage-like units presented in Fig. 2c. These H-units consist of 3 parallel layers of hydrogen atoms. Distances between hydrogen atoms in the first, second and third layers at 150 GPa are 1.07, 1.02 and 1.07 Å, respectively. These layers form 2D infinite networks. Each La atom in this structure is coordinated by 12 hydrogens with d_{La-H} = 2.05 Å at 150 GPa. The details of crystal structures of the predicted phases are summarized in Table S1 (see Supporting Information).

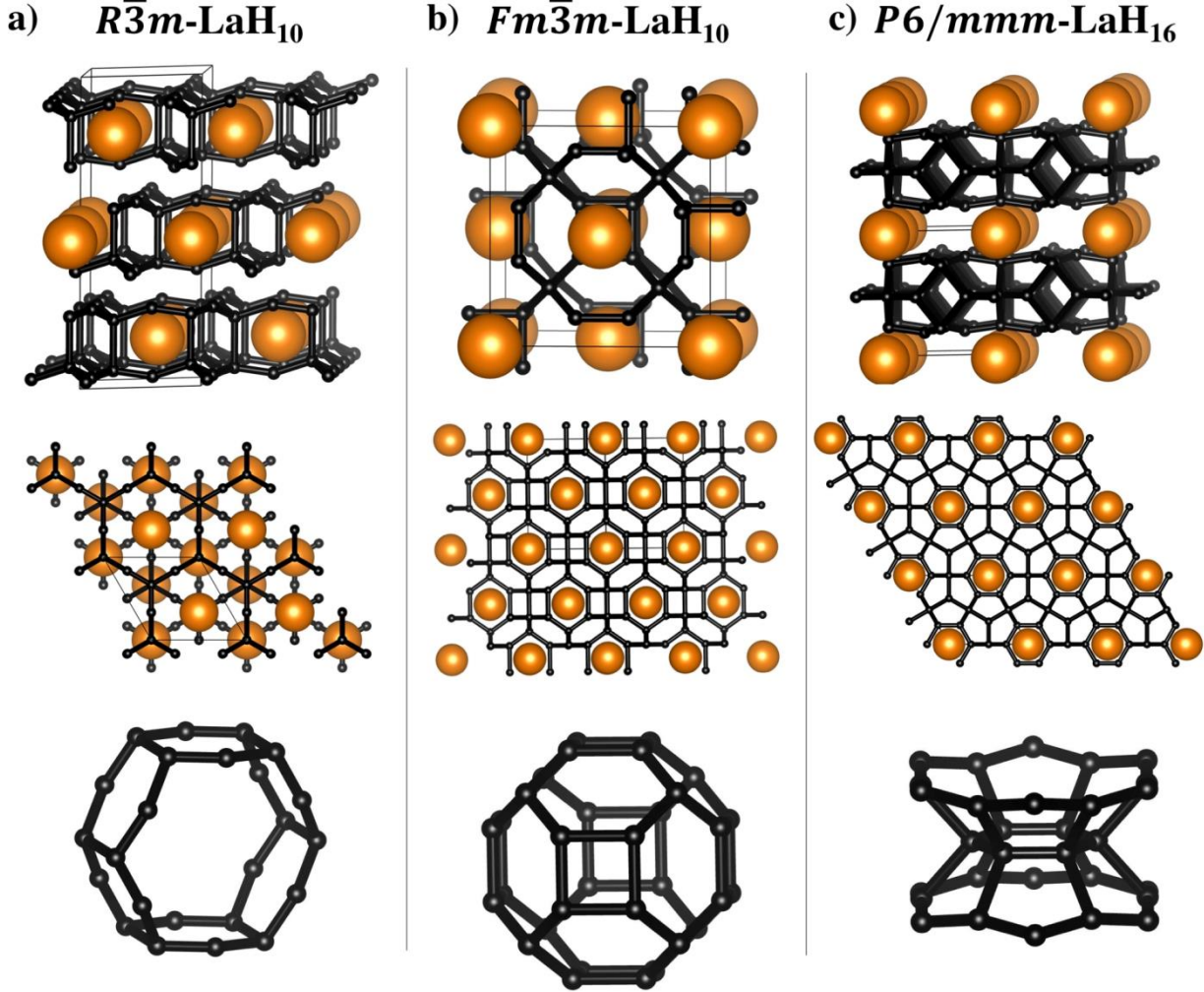


Fig. 2. Crystal structures of a) $R\bar{3}m$ -LaH₁₀, b) $Fm\bar{3}m$ -LaH₁₀ and c) $P6/mmm$ -LaH₁₆ at 150 GPa. In the first two rows different projections are shown. In the third row the typical hydrogen substructures are shown. Lanthanum atoms are shown by large orange balls, hydrogen atoms are black.

2. Raman scattering

Raman spectra of La+H₂ samples were investigated in Ref. [1] at pressures over 146 GPa. In the pressure range 155-170 GPa three groups of signals were detected: 810-840 cm⁻¹ ($d\omega_1/dP = 1.42$ cm⁻¹/GPa), 920-970 cm⁻¹ ($d\omega_2/dP = 2.39$ cm⁻¹/GPa) and 1255-1290 cm⁻¹ ($d\omega_3/dP = 2.28$ cm⁻¹/GPa). The authors associated these signals with the presence of LaH₃ phase [1]. Indeed, for instance, in Ref. [56] the LaH₃ was studied under pressure 0-45 GPa and the same set of signals was found: 510-810 cm⁻¹ ($d\omega_1/dP = 6.93$ cm⁻¹/GPa), 750-920 cm⁻¹ ($d\omega_2/dP = 8.19$ cm⁻¹/GPa) and 1050-1220 cm⁻¹ ($d\omega_3/dP = 5.24$ cm⁻¹/GPa). However, the extrapolation of these data to the high-pressure region around 170 GPa shows that all of these signals are no longer compatible with the experimentally observed ones from Ref. [1].

The second argument which questions the existence of LaH₃ in Raman spectra is that all similar metal-hydrogen compounds metalize long before 170 GPa with a complete disappearance of the Raman signal, as shown in experiments with ScH₃ [57] and YH₃ [58]. Probably the material found in Ref. [1] is a non-stoichiometric LaH_{3+x} phase or a solid solution. We analyzed the metallization process under pressure of the predicted lanthanum hydrides and found that $P\bar{1}$ -LaH₅ and $Cmc2_1$ -LaH₇ undergo the slowest metallization under pressure. Calculated Raman spectra for LaH₃, LaH₅, LaH₇, LaH₁₀ and LaH₁₆ at 170 GPa are shown in Fig. S5 (see Supporting Information) and the set

of signals of $Cmc2_1$ -LaH₇ is in the best agreement with experiment. Thus, in our opinion, the probability of formation of higher lanthanum hydrides should be taken into account.

3. Superconductivity

Next we performed a comprehensive study and analysis of possible superconducting state found in experiments [1,2]. Here we based mostly on the experimental results obtained by Drozdov et al. [1], because the synthesized sample by Somayazulu et al. [2] was obviously damaged by the laser heating and had low connectivity of the electrode system, which led to contradictory data on dT_C/dP and the appearance of artifacts in $R(T)$. But the transition to superconducting state at 245 K and 196 GPa is reliable and was taken into account for further analysis. Examination of the superconducting state in LaH₁₀ is based on the additional calculations of the Eliashberg functions $\alpha^2F(\omega)$ and electronic density of states for $R\bar{3}m$ and $Fm\bar{3}m$ -LaH₁₀ phases.

The main issue of any attempt of theoretical analysis is that $Fm\bar{3}m$ -LaH₁₀ is dynamically unstable below 200-210 GPa and EPC parameter λ increases to meaninglessly high values due to the divergence of $\alpha^2F(\omega)/\omega$ when $\omega \sim 0$. But the experimental observations describe the pressure regions from 100 to 200 GPa [1,2,17], where the cubic phase should be unstable at 0 K. At the first step we calculated the Eliashberg function for cubic $Fm\bar{3}m$ -LaH₁₀ at 200 GPa, shown in Fig. 3. Calculated parameters of superconducting transition at 200 GPa (see Table 1) are in good agreement with the data from Ref. [27], but slightly higher which is caused by the lower pressure.

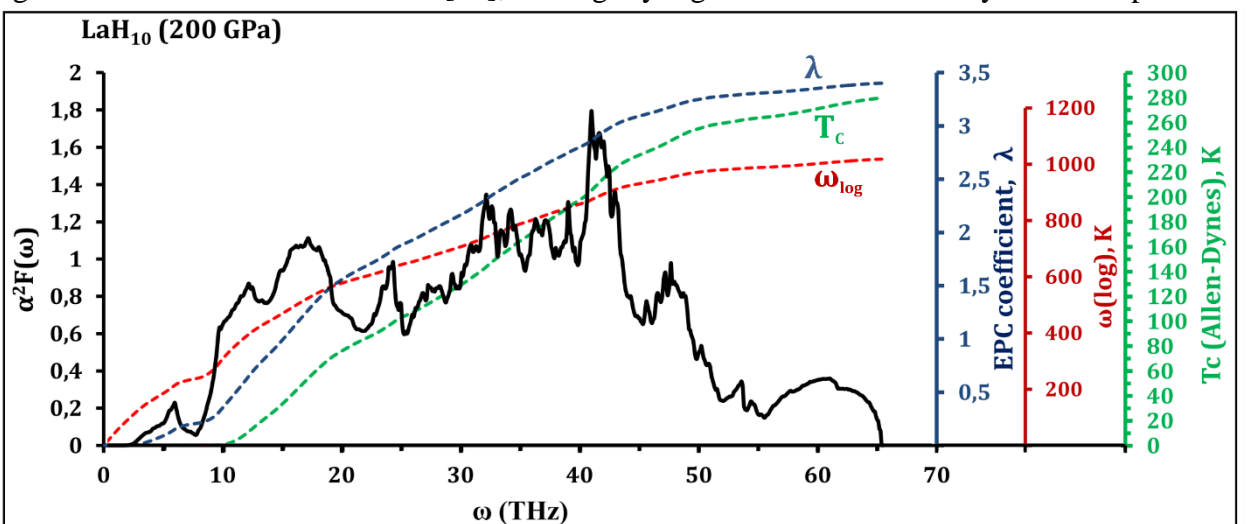


Fig. 3. Eliashberg function $\alpha^2F(\omega)$, ω_{\log} (red), EPC coefficient λ (blue), critical transition temperature (T_C) (green) of $Fm\bar{3}m$ -LaH₁₀ at 200 GPa.

Obtained data for $Fm\bar{3}m$ -LaH₁₀ including $\lambda = 3.39$ (210 GPa) and 2.26 (250 GPa), $\omega_{\log} = 852$ K, T_C (Eliashberg) = 271-283 K at $\mu^* = 0.1$ -0.13, and cell volume of 29 \AA^3 (250 GPa) together with density of electronic states $N(E_F) = N(0) = 10.6$ and 10.0 states/f.u./Ry at 200 and 250 GPa, respectively, allow us to estimate the Sommerfeld constant (see Table 1):

$$\gamma = \frac{2}{3} \pi^2 k_B^2 N(0)(1 + \lambda), \quad (5)$$

which is found to be 0.016 and 0.011 J/mol·K² at 200 and 250 GPa, respectively, that is close to Sommerfeld constant of $Fm\bar{3}m$ -ThH₁₀ (0.011 J/mol·K² [28], at 100 GPa). These constants were used to calculate $H_C(0)$ and ΔC in Table 1.

Processing of T_C data for LaH₁₀ [27] obtained by the exact solution of the Eliashberg equation for harmonic $\alpha^2F(\omega)$ gives average value of $dT_C/d\mu^* \approx -400$ K [27] in the pressure range 210-300 GPa and about -280 K for our data at 200 GPa. Using this derivative, we can roughly estimate the range of formal Coulomb pseudopotential μ^* , which would be in better agreement with the experimental T_C values of 215-245 K from Ref. [2]. Here we considered only the heating cycle from experiment [2]. The μ^* was calculated to be not less than 0.2-0.28 and not higher than 0.5-

0.7. From this point of view, it is appropriate to note this phenomenon of an anomalously large Coulomb pseudopotential, which was recently described for H_5S_2 [59,60]. For this reason, our results at 200 GPa (shown in Table 1) were supplemented by calculations with $\mu^* = 0.15, 0.2, 0.28$ and, sometimes, 0.7.

At this moment the anharmonic contribution and corresponding $\alpha^2 F(\omega)$ function are unknown. However, according to estimations of the anharmonic contribution in $c\text{II}4\text{-YH}_6$ at 120 GPa [61] it leads to decreasing of λ and increasing of ω_{\log} . As a result, critical temperature decreases by 34 K (from 288 K to 254 K), but this effect may not be sufficient to explain the difference in 71 K (decrease from 286 K to 215 K) for LaH_{10} in experimental works [1,2].

Table 1. Parameters of superconducting state of $Fm\bar{3}m\text{-LaH}_{10}$ at 200-250 GPa and $R\bar{3}m\text{-LaH}_{10}$ at 150 GPa. Here γ is Sommerfeld constant, μ^* is 0.15 (0.2), {0.28} and [0.1].

Parameter	$Fm\bar{3}m\text{-LaH}_{10}$			$R\bar{3}m\text{-LaH}_{10}$
	200 GPa	210 GPa	250 GPa	150 GPa
T_C , K	305 (289) {268} ^a	266	246	[223] 206
$\Delta(0)$, meV	73 (69) {63}	63.6	54	[53] 48
$H_C(0)$, T	100 (97) {92} ^b	85	74	[76] 72
$\Delta C/T_C$, mJ/mol·K ²	34.5 (38.6) {43}	30	34	[42] 45
γ , J/mol·K ²	0.016	0.016	0.011	0.016
$R_\Delta = 2\Delta(0)/k_B T_C$	5.55 {5.50}	5.55	5.1	[5.5] 5.4

^a Reducing the critical temperature to 213 K requires anomalously high $\mu^* = 0.7$. In this case, the critical magnetic field is ~ 76 T.

It is interesting to compare the experimentally obtained slope of the $T_C(P)$ function on the descending branch [1] with predicted values [27]. It can be determined from the T_C data [27] that $dT_C/dP = -0.355$ and -0.366 K/GPa ($\mu^* = 0.1$ and 0.13 , respectively) in the pressure range 200-300 GPa. Thus, the slope of $T_C(P)$ function depends on the Coulomb pseudopotential, and, for instance, at $\mu^* = 0.2\text{-}0.28$ the expected value of dT_C/dP is between -0.39 and -0.42 K/GPa, which is slightly higher than experimental value. However, as explained above, we could not take into account the factor of the difference in pressures (~ 50 GPa).

Measured value of dT_C/dP for LaH_{10} is -0.35 at 165 GPa [1], which is close to that of H_3S [62], and less than in Ref. [2] (-1 K/GPa at 192 GPa). It is noteworthy that the change of T_C by 10-20 K in the heating-cooling cycle with a pressure change from 188 to 196 GPa [2] contradicts the theoretical prediction by Niu et al. [27]. The value of dT_C/dP found in Ref. [1] is closer to the expected values according to our theoretical calculations. High values of $|dT_C/dP|$ in Ref. [2] may be due to the small variation in pressures ($\sim 4\%$), or proximity to the point of dynamical instability of the investigated LaH_{10} phase (compare T_C at 200 and 210 GPa in Table 1).

Further investigation of superconductivity in $Fm\bar{3}m\text{-LaH}_{10}$ implies the synthesis of lanthanum deuteride LaD_{10} and determination of the isotopic coefficient. The expected isotopic coefficient calculated using the McMillan formula can be expressed as

$$\beta = -\frac{d \ln T_C}{d \ln M} = \frac{1}{2} \left[1 - \frac{1.04(1+\lambda)(1+0.62\lambda)}{[\lambda - \mu^*(1+0.62\lambda)]^2} \mu^{*2} \right] \quad (6)$$

and is equal to 0.41-0.46 (based on the data from Ref. [27]) for LaH_{10} at 210 GPa. Using the isotopic coefficient β one can determine the critical temperature of lanthanum decadeuteride ($Fm\bar{3}m\text{-LaD}_{10}$) as $T_D = 2^\beta \cdot T_C = 156\text{-}184$ K. Also β decreases down to 0.36-0.41 with increasing of μ^* up to 0.28-0.33.

Further study of superconductivity in LaH_{10} implies investigation of the behavior of samples in a magnetic field. Using semi-empirical equations of the BCS theory (see Ref. [63], equations 5.11 and 5.9):

$$\frac{\gamma T_c^2}{H_c^2(0)} = 0.168 \left[1 - 12.2 \left(\frac{T_c}{\omega_{\log}} \right)^2 \ln \left(\frac{\omega_{\log}}{3T_c} \right) \right] \quad (7)$$

and

$$\frac{\Delta C(T_c)}{\gamma T_c} = 1.43 \left[1 + 53 \left(\frac{T_c}{\omega_{\log}} \right)^2 \ln \left(\frac{\omega_{\log}}{3T_c} \right) \right], \quad (8)$$

we estimated the upper critical magnetic field, and the jump in specific heat for $Fm\bar{3}m$ -LaH₁₀ (see Table 1). Estimation of the upper critical magnetic field gives $H_c(0) = 76$ -100 T at 200-210 GPa, which exceeds that for H₃S (~70 T) [62] due to a higher electron density and a higher EPC parameter.

As was proposed earlier, results obtained by Drozdov et al. [1] can be related to the properties of $R\bar{3}m$ -LaH₁₀ (due to the considered pressure region). Thus, we calculated the Eliashberg function and the parameters of the superconducting state for $R\bar{3}m$ -LaH₁₀ at 150 GPa (see Tables 1-2). Calculated critical temperature is found to be 206-223 K (for $\mu^* = 0.1$ -0.15), which is sufficiently lower than for $Fm\bar{3}m$ ($T_c > 286$ K) and well agrees with experimental value measured by Drozdov et al. [1]. Isotopic coefficient for $R\bar{3}m$ -LaH₁₀ calculated by McMillan formula is 0.47-0.49 ($\mu^* = 0.1$ -0.15), which leads to $T_c(R\bar{3}m\text{-LaD}_{10}) = 149$ -159 K, critical magnetic field of 76 T. Thus, one can distinguish between $R\bar{3}m$ and $Fm\bar{3}m$ lanthanum decahydrides based on the measured superconducting properties.

Moving to the discussion of newly predicted $P6/mmm$ -LaH₁₆ it should be noticed that there was no PXRD signature found in experimental study [17], because peaks from LaH₁₆ should appear at lower angles compared to LaH₁₀. This fact may indicate that LaH₁₆ should appear at higher pressures from 200 to 250 GPa, despite of thermodynamic stability from 150 GPa (see Fig. 1) and dynamical stability from 200 GPa (see Supporting Information for details).

Study of the electronic properties of $P6/mmm$ -LaH₁₆ in the pressure range 200-300 GPa (shown in Fig. 4a) displays that electronic density of states is insensible to pressure. Both intra and interlayered conductivity is caused by the *n*-doped hydrogen sublattice as can be seen from the atom-projected band structure, Fig. 4b.

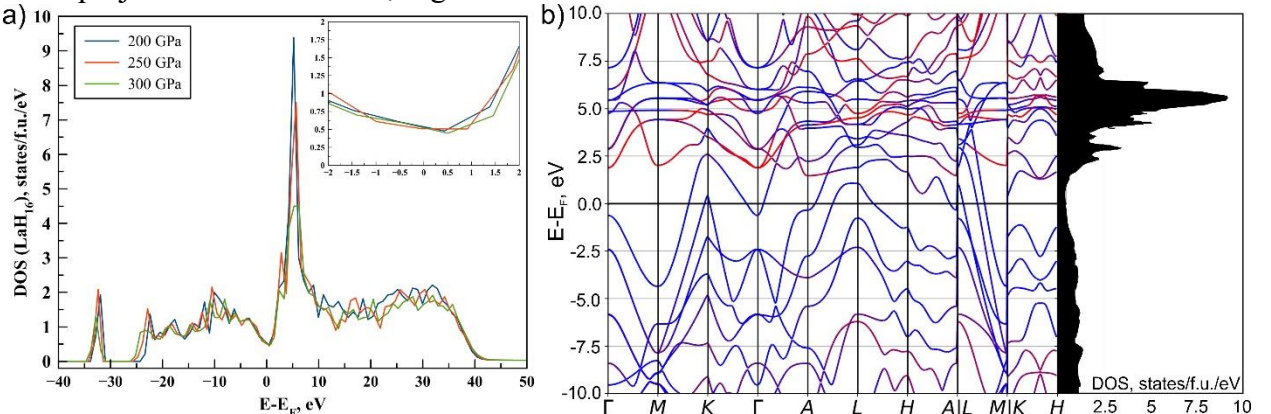


Fig. 4. a) Calculated electronic DOS for $P6/mmm$ -LaH₁₆ at 200, 250 and 300 GPa (the inset contains DOS near E_F); b) band structure and DOS of LaH₁₆ (red curves – La, blue - H) at 250 GPa.

The computed Eliashberg function for $P6/mmm$ -LaH₁₆ at the lowest investigated pressure 200 GPa is shown in Fig. 5a (see Supporting Information for other pressures). The comparison of obtained data with the previously studied $Fm\bar{3}m$ -LaH₁₀ (see Table 2) shows that the EPC parameter of LaH₁₆ $\lambda = 1.4 - 1.8$ is approximately 2 times lower than that of LaH₁₀, which leads to the higher sensitivity to Coulomb pseudopotential ($dT_c/d\mu^*$) in LaH₁₆. But the rapid increase of ω_{\log} with pressure (see Fig. 5b) leads to the weak dependence of T_c (from 231 to 248 K) on the pressure with $dT_c/dP = -0.17$ K/GPa. Absolute values of T_c are lower than for $Fm\bar{3}m$ -LaH₁₀ at the same pressure range and with the same μ^* . Increasing of the value of Coulomb pseudopotential to 0.2-0.28 leads to a decrease of T_c to 146-195 K.

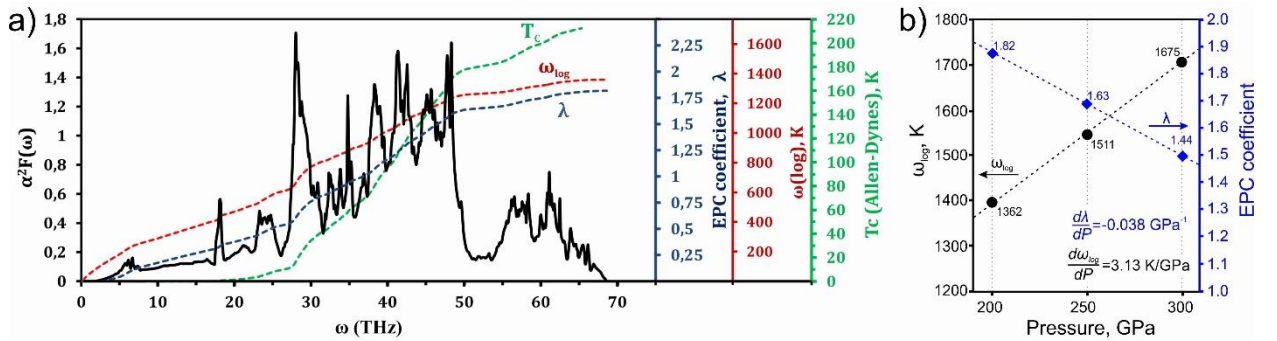


Fig. 5. a) Eliashberg function $\alpha^2 F(\omega)$ (black), ω_{\log} (red), EPC coefficient λ (blue) and critical transition temperature (T_C , green) of $P6/mmm$ -LaH₁₆ at 200 GPa; b) dependence of EPC parameter and ω_{\log} on pressure.

Several additional parameters of the superconducting state of $P6/mmm$ -LaH₁₆, including upper critical field, jump in specific heat and superconductive gap, are shown in Table 3. Following our calculations upper critical magnetic field decreases with T_C down to $H_C \sim 50$ T. The superconductive gap was estimated by well-known semi-empirical equation, working satisfactorily for $T_C/\omega_{\log} < 0.25$ (see equation 4.1 in Ref. [63]):

$$\frac{2\Delta(0)}{k_B T_C} = 3.53 \left[1 + 12.5 \left(\frac{T_C}{\omega_{\log}} \right)^2 \ln \left(\frac{\omega_{\log}}{2T_C} \right) \right]. \quad (9)$$

Table 2. Predicted superconducting properties of lanthanum hydrides. T_C values are given for μ^* equal to 0.1, while T_C in brackets are for $\mu^* = 0.15$.

Phase	P , GPa	λ	N_f , states/f.u./Ry	ω_{\log} , K	T_C (McMillan), K	T_C (Allen-Dynes), K	T_C (Eliashberg), K
$Fm\bar{3}m$ -LaH ₁₀	200	3.4	10.6	1018	193 (178)	279 (258)	326 (305)
	210	3.41	10.0	848	238 ^a (219) ^a	-	286 (266 ^b)
$R\bar{3}m$ -LaH ₁₀	150	2.77	12.2	833	144 (132)	197 (171)	223 (206)
$P6/mmm$ -LaH ₁₆	200	1.82	7.21	1362	183 (160)	215 (189)	248 (226)
	250	1.63	6.94	1511	186 (161)	213.6 (180)	243 (219)
	300	1.44	7.07	1675	183 (155)	205 (174)	231 (205)

^a According to MacMillan equation $\exp \left(-\frac{1.04(1+\lambda)}{\lambda - \mu^* - 0.62\lambda\mu^*} \right) = 0.227$ and with $\omega_{\log} = 848$ K (see Table S1 in Ref. [27])

-should be 161 (149) K

^b Expected values based on linear extrapolation from Ref. [27].

In order to be sure of the obtained results, we compared values calculated by semi-empirical formulas (7)-(9) [63] and P. Allen's algorithm [64] for $T_C(E)$ (see Supporting Information) with the precise numerical solution of Eliashberg equations for $P6/mmm$ -LaH₁₆ at 250 GPa (Table 3, "exact solution"). Calculations show excellent agreement between semi-empirical and the precise numerical method.

Table 3. Parameters of superconductive state in $P6/mmm$ -LaH₁₆ at 200-300 GPa. Here γ is Sommerfeld constant (calculated by eq. (5)), μ^* is 0.1 (0.15).

Parameter	$P6/mmm$ -LaH ₁₆			
	200 GPa	250 GPa Semi-empirical	250 GPa Exact solution	300 GPa
T_C , K	248 (226)	243 (219)	241 (212)	231 (205)
$\Delta(0)$, meV	53.5 (47)	50.5 (44)	46.4 (40)	46 (39)
$H_C(0)$, T	58 (53)	53.6 (48)	52.3 (46)	49 (43)
$\Delta C/T_C$, mJ/mol·K ²	20.6 (20)	18 (17)	17.3 (17.2)	16 (15.4)
γ , J/mol·K ²	0.007	0.0063	0.0063	0.006
$R_\Delta = 2\Delta(0)/k_B T_C$	5 (4.9)	4.8 (4.7)	4.5 (4.4)	4.6 (4.5)

Conclusions

Here we performed crystal structure search using evolutionary algorithm USPEX in the La-H system at 50 and 150 GPa. Obtained results for the stable phases and crystal structure of LaH₁₀ agree with previous findings [12,17]. However, we predict new thermodynamically stable metallic superhydride $P6/mmm$ -LaH₁₆. This phase is a high-temperature superconductor with T_C of 219-243 K depending on μ^* , upper critical magnetic field of ~ 50 T and superconducting gap of 50 meV. The critical magnetic field for $Fm\bar{3}m$ -LaH₁₀ was found to be 76-100 T and lower 76 T for $R\bar{3}m$ modification. We also estimated the critical temperature for $Fm\bar{3}m$ -LaD₁₀ (156-184 K) and $R\bar{3}m$ -LaD₁₀ (149-159 K) which corresponds to the isotopic coefficients $\beta = 0.41$ -0.46 and 0.47-0.49 respectively. Considering all the data we can conclude about the critical role of the Coulomb pseudopotential for LaH_{10+x}, which is expected to have anomalously large values ≥ 0.2 -0.28 in order to describe experimental data. Alternatively, the possible explanation of the experimental results is that measurements by Drozdov et al. [1] were performed for $R\bar{3}m$ -LaH₁₀ with $T_C = 206$ -223 K, while measurements by Somayazulu et al. [2] were made for cubic $Fm\bar{3}m$ modification of lanthanum decahydride with critical temperature higher than 280 K.

Acknowledgements

The work was supported by Russian Science Foundation (№ 16-13-10459). Calculations were performed on the Rurik supercomputer at MIPT. The authors express their gratitude to Izabela Wrona (Czestochowa Univ., Inst. of Phys.) for help in preparing the manuscript. A.G.K. thanks to FASIE foundation for financial support within UMNIK grant №13408GU/2018.

References

- [1] A. P. Drozdov, V. S. Minkov, S. P. Besedin, P. P. Kong, M. A. Kuzovnikov, D. A. Knyazev, and M. I. Eremets, ArXiv180807039 Cond-Mat (2018).
- [2] M. Somayazulu, M. Ahart, A. K. Mishra, Z. M. Geballe, M. Baldini, Y. Meng, V. V. Struzhkin, and R. J. Hemley, ArXiv180807695 Cond-Mat (2018).
- [3] N. W. Ashcroft, Phys. Rev. Lett. **21**, 1748 (1968).
- [4] P. Cudazzo, G. Profeta, A. Sanna, A. Floris, A. Continenza, S. Massidda, and E. K. U. Gross, Phys. Rev. B **81**, 134505 (2010).
- [5] R. P. Dias and I. F. Silvera, Science eaal1579 (2017).
- [6] N. W. Ashcroft, Phys. Rev. Lett. **92**, 187002 (2004).
- [7] H. Wang, J. S. Tse, K. Tanaka, T. Iitaka, and Y. Ma, Proc. Natl. Acad. Sci. **109**, 6463 (2012).
- [8] Y. Chen, Q.-M. Hu, and R. Yang, Phys. Rev. Lett. **109**, 157004 (2012).
- [9] D. Duan, Y. Liu, F. Tian, D. Li, X. Huang, Z. Zhao, H. Yu, B. Liu, W. Tian, and T. Cui, Sci. Rep. **4**, 6968 (2014).
- [10] A. G. Kvashnin, D. V. Semenok, I. A. Kruglov, and A. R. Oganov, ArXiv:1711.00278 <http://arxiv.org/abs/1711.00278> (2017).

- [11] D. V. Semenok, A. G. Kvashnin, I. A. Kruglov, and A. R. Oganov, *J. Phys. Chem. Lett.* **9**, 1920 (2018).
- [12] H. Liu, I. I. Naumov, R. Hoffmann, N. W. Ashcroft, and R. J. Hemley, *Proc. Natl. Acad. Sci.* **114**, 6990 (2017).
- [13] A. P. Drozdov, M. I. Eremets, I. A. Troyan, V. Ksenofontov, and S. I. Shylin, *Nature* **525**, 73 (2015).
- [14] D. Duan, Y. Liu, Y. Ma, Z. Shao, B. Liu, and T. Cui, *Natl. Sci. Rev.* **4**, 121 (2017).
- [15] A. K. Mishra, M. Somayazulu, M. Ahart, A. Karandikar, R. J. Hemley, and V. V. Struzhkin, in *Bull. Am. Phys. Soc.* (2018).
- [16] P. P. Kong, A. P. Drozdov, E. Eroke, and M. I. Eremets, in *Book Abstr. AIRAPT 26 Jt. ACHPR 8 CHPC 19* (Beijing, China, 2017), p. 347.
- [17] Z. M. Geballe, H. Liu, A. K. Mishra, M. Ahart, M. Somayazulu, Y. Meng, M. Baldini, and R. J. Hemley, *Angew. Chem. Int. Ed.* **57**, 688 (2017).
- [18] C. M. Pépin, G. Geneste, A. Dewaele, M. Mezouar, and P. Loubeyre, *Science* **357**, 382 (2017).
- [19] A. Majumdar, J. S. Tse, M. Wu, and Y. Yao, *Phys. Rev. B* **96**, 201107 (2017).
- [20] A. G. Kvashnin, I. A. Kruglov, D. V. Semenok, and A. R. Oganov, *J. Phys. Chem. C* **122**, 4731 (2018).
- [21] I. A. Kruglov, A. G. Kvashnin, A. F. Goncharov, A. R. Oganov, S. Lobanov, N. Holtgrewe, and A. V. Yanilkin, ArXiv:1708.05251 <https://arxiv.org/abs/1708.05251>, (2017).
- [22] N. P. Salke, M. M. D. Esfahani, Y. Zhang, I. A. Kruglov, J. Zhou, Y. Wang, E. Greenberg, V. B. Prakapenka, A. R. Oganov, and J.-F. Lin, ArXiv:1805.02060 <https://arxiv.org/ftp/arxiv/papers/1805/1805.02060.pdf> (2018).
- [23] H. Wang, J. S. Tse, K. Tanaka, T. Iitaka, and Y. Ma, *Proc. Natl. Acad. Sci.* **109**, 6463 (2012).
- [24] K. Tanaka, J. S. Tse, and H. Liu, *Phys. Rev. B* **96**, 100502 (2017).
- [25] G. Gao, R. Hoffmann, N. W. Ashcroft, H. Liu, A. Bergara, and Y. Ma, *Phys. Rev. B* **88**, 184104 (2013).
- [26] K. Abe, *Phys. Rev. B* **96**, 144108 (2017).
- [27] X. Li and F. Peng, *Inorg. Chem.* **56**, 13759 (2017).
- [28] A. G. Kvashnin, D. V. Semenok, I. A. Kruglov, and A. R. Oganov, *Phys Rev Lett* **Submitted**, (2018).
- [29] G. M. Eliashberg, *JETP* **11**, 696 (1959).
- [30] A. B. Migdal, *JETP* **34**, 996 (1958).
- [31] A. P. Drozdov, V. S. Minkov, S. P. Besedin, P. P. Kong, M. A. Kuzovnikov, D. A. Knyazev, and M. I. Eremets, ArXiv180807039 Cond-Mat (2018).
- [32] M. Somayazulu, M. Ahart, A. K. Mishra, Z. M. Geballe, M. Baldini, Y. Meng, V. V. Struzhkin, and R. J. Hemley, ArXiv180807695 Cond-Mat (2018).
- [33] A. R. Oganov and C. W. Glass, *J Chem Phys* **124**, 244704 (2006).
- [34] C. W. Glass, A. R. Oganov, and N. Hansen, *Comput. Phys. Commun.* **175**, 713 (2006).
- [35] A. O. Lyakhov, A. R. Oganov, H. T. Stokes, and Q. Zhu, *Comput. Phys. Commun.* **184**, 1172 (2013).
- [36] P. Hohenberg and W. Kohn, *Phys Rev* **136**, B864 (1964).
- [37] W. Kohn and L. J. Sham, *Phys Rev* **140**, A1133 (1965).
- [38] J. P. Perdew, K. Burke, and M. Ernzerhof, *Phys. Rev. Lett.* **77**, 3865 (1996).
- [39] P. E. Blöchl, *Phys. Rev. B* **50**, 17953 (1994).
- [40] G. Kresse and D. Joubert, *Phys. Rev. B* **59**, 1758 (1999).
- [41] G. Kresse and J. Furthmüller, *Phys. Rev. B* **54**, 11169 (1996).
- [42] G. Kresse and J. Hafner, *Phys. Rev. B* **47**, 558 (1993).
- [43] G. Kresse and J. Hafner, *Phys. Rev. B* **49**, 14251 (1994).
- [44] A. Rossi, *Nature* **133**, 174 (1934).
- [45] C. J. Pickard and R. J. Needs, *Nat. Phys.* **3**, 473 (2007).
- [46] P. Giannozzi, S. Baroni, N. Bonini, M. Calandra, R. Car, C. Cavazzoni, D. Ceresoli, G. L.

Chiarotti, M. Cococcioni, I. Dabo, A. D. Corso, S. de Gironcoli, S. Fabris, G. Fratesi, R. Gebauer, U. Gerstmann, C. Gouguassis, A. Kokalj, M. Lazzeri, L. Martin-Samos, N. Marzari, F. Mauri, R. Mazzarello, S. Paolini, A. Pasquarello, L. Paulatto, C. Sbraccia, S. Scandolo, G. Sclauzero, A. P. Seitsonen, A. Smogunov, P. Umari, and R. M. Wentzcovitch, *J. Phys. Condens. Matter* **21**, 395502 (2009).

[47] S. Baroni, S. de Gironcoli, A. Dal Corso, and P. Giannozzi, *Rev. Mod. Phys.* **73**, 515 (2001).

[48] A. Togo and I. Tanaka, *Scr. Mater.* **108**, 1 (2015).

[49] A. Togo, F. Oba, and I. Tanaka, *Phys. Rev. B* **78**, 134106 (2008).

[50] L. P. Gor'kov, *JETP* **34**, 735 (1958).

[51] E. G. Maksimov, D. Y. Savrasov, and S. Y. Savrasov, *Phys.-Uspekhi* **40**, 337 (1997).

[52] P. B. Allen and R. C. Dynes, *Phys. Rev. B* **12**, 905 (1975).

[53] K. Momma and F. Izumi, *J. Appl. Crystallogr.* **44**, 1272 (2011).

[54] I. A. Kruglov, A. G. Kvashnin, A. F. Goncharov, A. R. Oganov, S. S. Lobanov, N. Holtgrewe, S. Jiang, V. B. Prakapenka, E. Greenberg, and A. V. Yanilkin, *Sci Adv* **Just Accepted**, (2018).

[55] D. V. Semenok, I. A. Kruglov, A. G. Kvashnin, and A. R. Oganov, *ArXiv180600865 Cond-Mat* (2018).

[56] H. Meng, M. A. Kuzovnikov, and M. Tkacz, *Int. J. Hydrog. Energy* **42**, 29344 (2017).

[57] T. Kume, H. Ohura, T. Takeichi, A. Ohmura, A. Machida, T. Watanuki, K. Aoki, S. Sasaki, H. Shimizu, and K. Takemura, *Phys. Rev. B* **84**, 064132 (2011).

[58] T. Kume, H. Ohura, S. Sasaki, H. Shimizu, A. Ohmura, A. Machida, T. Watanuki, K. Aoki, and K. Takemura, *Phys. Rev. B* **76**, 024107 (2007).

[59] I. Kruglov, R. Akashi, S. Yoshikawa, A. R. Oganov, and M. M. D. Esfahani, *Phys. Rev. B* **96**, 220101 (2017).

[60] M. Kostrzewska, R. Szcześniak, J. K. Kalaga, and I. A. Wrona, *ArXiv180409760 Cond-Mat* (2018).

[61] A. Bergara, in *Proc. 56th EPRG Meet.* (Aveiro, 2018).

[62] A. P. Drozdov, M. I. Eremets, I. A. Troyan, V. Ksenofontov, and S. I. Shylin, *Nature* **525**, 73 (2015).

[63] J. P. Carbotte, *Rev. Mod. Phys.* **62**, 1027 (1990).

[64] P. B. Allen and R. C. Dynes, *Tech. Rep. 7 TCM41974* (1974).

Supporting Information

Superconductivity in LaH₁₀: a new twist of the story

Ivan A. Kruglov,^{1,2,} Dmitrii V. Semenok,^{1,3} Radosław Szcześniak,^{4,5} M. Mahdi Davari Esfahani,⁶ Alexander G. Kvashnin^{3,1} and Artem R. Oganov,^{3,2,7}*

¹ Moscow Institute of Physics and Technology, 141700, 9 Institutsky lane, Dolgoprudny, Russian Federation

² Dukhov Research Institute of Automatics (VNIIA), Moscow 127055, Russian Federation

³ Skolkovo Institute of Science and Technology, Skolkovo Innovation Center 143026, 3 Nobel Street, Moscow, Russian Federation

⁴ Institute of Physics, Jan Dlugosz University in Czestochowa, Ave. Armii Krajowej 13/15, 42-200 Czestochowa, Poland

⁵ Institute of Physics, Częstochowa University of Technology, Ave. Armii Krajowej 19, 42-200 Częstochowa, Poland

⁶ Department of Geosciences and Center for Materials by Design, Institute for Advanced Computational Science, State University of New York, Stony Brook, NY 11794-2100, USA

⁷ International Center for Materials Discovery, Northwestern Polytechnical University, Xi'an, 710072, China

Corresponding Author

*Ivan Kruglov, E-mail: ivan.kruglov@phystech.edu

Content

Equations for calculating T_C	15
Raman spectra.....	18
Electronic and phonon properties of La-H phases.....	19
Eliashberg spectral functions	24
Matlab functions for T_C calculation using Allen's algorithm from Ref. 3	26
References.....	28

Crystal data of La-H phases

Table S1. Crystal structures of predicted La-H phases.

Phase	Pressure, GPa	Lattice parameters	Coordinates			
<i>Fm</i> $\bar{3}m$ -LaH	50	$a = 4.53 \text{ \AA}$	La	0.5	0.5	0.5
			H	0.0	0.0	0.0
<i>Pnma</i> -LaH ₃	50	$a = 7.20 \text{ \AA}$, $b = 4.57 \text{ \AA}$, $c = 3.67 \text{ \AA}$	La	-0.365	0.25	-0.320
			H	0.394	-0.001	-0.171
			H	0.356	0.25	0.332
<i>Cmc2</i> ₁ -LaH ₇	50	$a = 7.20 \text{ \AA}$, $b = 4.57 \text{ \AA}$, $c = 3.67 \text{ \AA}$	La	0.0	-0.159	-0.452
			H	0.0	0.466	0.408
			H	0.0	0.245	-0.300
			H	0.0	-0.365	0.241
			H	0.0	0.174	0.420
			H	0.25	0.417	0.237
			H	0.0	-0.497	-0.465
<i>P6/mmm</i> - LaH ₂	150	$a = 2.80 \text{ \AA}$, $c = 2.72 \text{ \AA}$	La	0.0	0.0	0.0
			H	0.333	0.667	0.5
<i>Cmcm</i> -LaH ₃	150	$a = 2.76 \text{ \AA}$, $b = 10.69 \text{ \AA}$, $c = 2.80 \text{ \AA}$	La	0.0	0.118	0.25
			H	0.0	0.467	0.25
			H	0.0	0.313	0.25
			H	0.0	-0.25	0.25
<i>Cmmm</i> -La ₃ H ₁₀	150	$a = 16.70 \text{ \AA}$, $b = 2.77 \text{ \AA}$, $c = 2.75 \text{ \AA}$	La	-0.326	0.0	0.5
			La	0.0	0.0	0.0
			H	-0.089	0.0	0.5
			H	0.128	0.0	0.0
			H	-0.228	0.0	0.0
			H	-0.449	0.0	0.5
			H	0.411	0.0	0.0
<i>I4/mmm</i> -LaH ₄	150	$a = 2.74 \text{ \AA}$, $c = 6.03 \text{ \AA}$	La	0.0	0.0	0.5
			H	0.0	0.5	0.25
			H	0.0	0.0	-0.153
<i>P</i> $\bar{1}$ -LaH ₅	150	$a = 2.91 \text{ \AA}$, $b = 5.26 \text{ \AA}$, $c = 3.47 \text{ \AA}$, $\alpha = 93.34$, $\beta = 110.24$, $\gamma = 98.71$	La	-0.327	-0.266	-0.273
			H	0.263	0.036	-0.255
			H	0.073	0.431	-0.280
			H	-0.067	0.122	-0.349
			H	-0.304	0.375	-0.108
			H	-0.376	0.112	-0.151
<i>R</i> $\bar{3}m$ -LaH ₁₀	150	$a = 3.66 \text{ \AA}$, $c = 8.53 \text{ \AA}$	La	0.0	0.0	0.5
			H	0.0	0.0	0.097
			H	-0.168	0.168	0.276
			H	0.0	0.0	-0.259
<i>Fm</i> $\bar{3}m$ -LaH ₁₀	150	$a = 5.08 \text{ \AA}$	La	0.0	0.0	0.0
			H	-0.378	-0.378	-0.378
			H	0.25	0.25	0.25
<i>P6/mmm</i> - LaH ₁₆	150	$a = 3.68 \text{ \AA}$, $c = 3.70 \text{ \AA}$	La	0.0	0.0	0.0
			H	-0.276	0.0	0.5
			H	0.5	0.0	0.245
			H	0.333	0.667	-0.203

Equations for calculating T_C

The critical temperature of superconducting transition was calculated using Matsubara-type linearized Eliashberg equations:¹

$$\hbar\omega_j = \pi(2j+1) \cdot k_B T, \quad j = 0, \pm 1, \pm 2, \dots \quad (S1)$$

$$\lambda(\omega_i - \omega_j) = 2 \int_0^\infty \frac{\omega \cdot \alpha^2 F(\omega)}{\omega^2 + (\omega_i - \omega_j)^2} d\omega \quad (S2)$$

$$\Delta(\omega = \omega_i, T) = \Delta_i(T) = \pi k_B T \sum_j \frac{[\lambda(\omega_i - \omega_j) - \mu^*]}{\rho + \left| \hbar\omega_j + \pi k_B T \sum_k (\text{sign} \omega_k) \cdot \lambda(\omega_j - \omega_k) \right|} \cdot \Delta_j(T) \quad (S3)$$

where T is temperature in Kelvins, μ^* is Coulomb pseudopotential, ω is frequency in Hz, $\rho(T)$ is a pair-breaking parameter, function $\lambda(\omega_i - \omega_j)$ relates to effective electron-electron interaction via exchange of phonons.² Transition temperature can be found as a solution of equation $\rho(T_C) = 0$ where $\rho(T)$ is defined as $\max(\rho)$ providing that $\Delta(\omega)$ is not a zero function of ω at fixed temperature.

These equations can be rewritten in a matrix form as³

$$\rho(T) \psi_m = \sum_{n=0}^N K_{mn} \psi_n \Leftrightarrow \rho(T) \begin{pmatrix} \psi_1 \\ \dots \\ \psi_N \end{pmatrix} = \begin{pmatrix} K_{11} & \dots & K_{1N} \\ \dots & K_{ii} & \dots \\ K_{N1} & \dots & K_{NN} \end{pmatrix} \times \begin{pmatrix} \psi_1 \\ \dots \\ \psi_N \end{pmatrix}, \quad (S4)$$

where ψ_n relates to $\Delta(\omega, T)$, and

$$K_{mn} = F(m-n) + F(m+n+1) - 2\mu^* - \delta_{mn} \left[2m+1 + F(0) + 2 \sum_{l=1}^m F(l) \right] \quad (S5)$$

$$F(x) = F(x, T) = 2 \int_0^{\omega_{\max}} \frac{\alpha^2 F(\omega)}{(\hbar\omega)^2 + (2\pi \cdot kT \cdot x)^2} \hbar^2 \omega d\omega, \quad (S6)$$

where $\delta_{nn} = 1$ and $\delta_{nm} = 0$ ($n \neq m$) – is a unit matrix. Now one can replace criterion of $\rho(T_C) = 0$ by the vanishing of the maximum eigenvalue of the matrix K_{nm} : $\{\rho = \max_{\text{eigenvalue}}(K_{nm}) = f(T), f(T_C) = 0\}$.

We have implemented this simple approach, proposed by Philip Allen in 1974, as Matlab functions, shown at the last page of Supporting Information, which read files with $\alpha^2 F$ functions and carry out the calculations of T_C .

Exact calculations for *P6/mmm*-LaH₁₆ at 250 GPa were also made using the Eliashberg equations in the following form (on the imaginary axis):¹

$$\phi_n = \frac{\pi}{\beta} \sum_{m=-M}^M \frac{\lambda(i\omega_n - i\omega_m) - \mu^* \theta(\omega_c - |\omega_m|)}{\sqrt{(\hbar\omega_m Z_m)^2 + \phi_m^2}} \phi_m \quad (S7)$$

$$Z_n = 1 + \frac{1}{\omega_n} \frac{\pi}{\beta} \sum_{m=-M}^M \frac{\lambda(i\omega_n - i\omega_m)}{\sqrt{(\hbar\omega_m Z_m)^2 + \phi_m^2}} \omega_m Z_m \quad (S8)$$

where: ϕ_n is the order parameter function, Z_n is the wave function renormalization factor, $\theta(x)$ is Heaviside function, $\hbar\omega_n = \pi \cdot k_B T \cdot (2n-1)$ is the n -th Matsubara frequency, $\beta = 1/k_B T$, μ^* is Coulomb pseudopotential, ω_c is the cut-off energy ($\omega_c = 3\Omega_{\max}$, Ω_{\max} is the maximum frequency in $\alpha^2 F(\omega)$). The electron-phonon pairing kernel is defined as:

$$\lambda(z) = 2 \int_0^{\Omega_{\max}} \frac{\alpha^2 F(\Omega)}{\Omega^2 - z^2} \Omega d\Omega. \quad (S9)$$

The Eliashberg equations have been solved for 2201 Matsubara frequencies, starting from $T_0 = 10$ K (below this temperature, the solutions are not stable). The methods discussed in the papers⁴⁻⁶ were used during the calculations.

The full form of the order parameter and the wave function renormalization factor on the real axis was obtained through analytical extension of the Eliashberg equations solutions from the imaginary axis, using the formula:

$$X(\omega) = \frac{p_1 + p_2\omega + \dots + p_r\omega^{r-1}}{q_1 + q_2\omega + \dots + q_r\omega^{r-1} + \omega^r}, \quad (S10)$$

where $X \in \{\Delta; Z\}$, $r = 50$. The values of p_j and q_j parameters were selected in accordance with the principles presented at work.⁷ Obtained results allow one to calculate dimensionless parameter R_C (relative jump of the specific heat), using the formula below:

$$R_C = \frac{C^S(T_C) - C^N(T_C)}{C^N(T_C)} \quad (S11)$$

Because of strong-coupling and retardation effects in LaH₁₀ and LaH₁₆, parameter R_C differs significantly from BCS theory prediction, in which the constant value is equal to 1.43.⁸

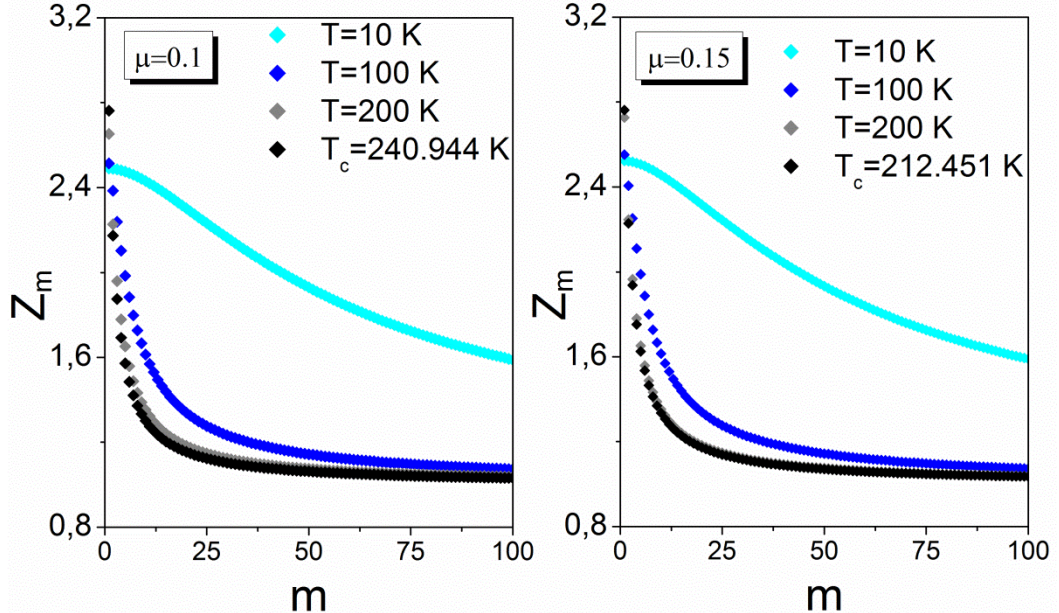


Fig. S1. The wave function renormalization factor for $P6/mmm$ -LaH₁₆ at 250 GPa on the imaginary axis for the selected values of temperature (the first 100 values).

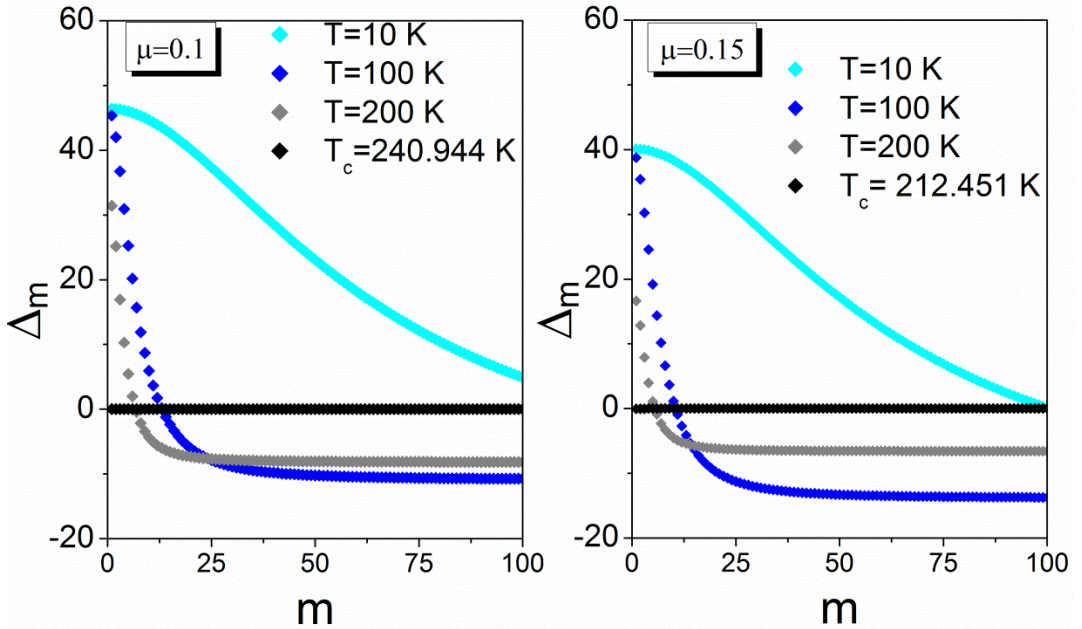


Fig. S2. The order parameter (in meV) for $P6/mmm$ -LaH₁₆ at 250 GPa on the imaginary axis for the selected values of temperature (the first 100 values).

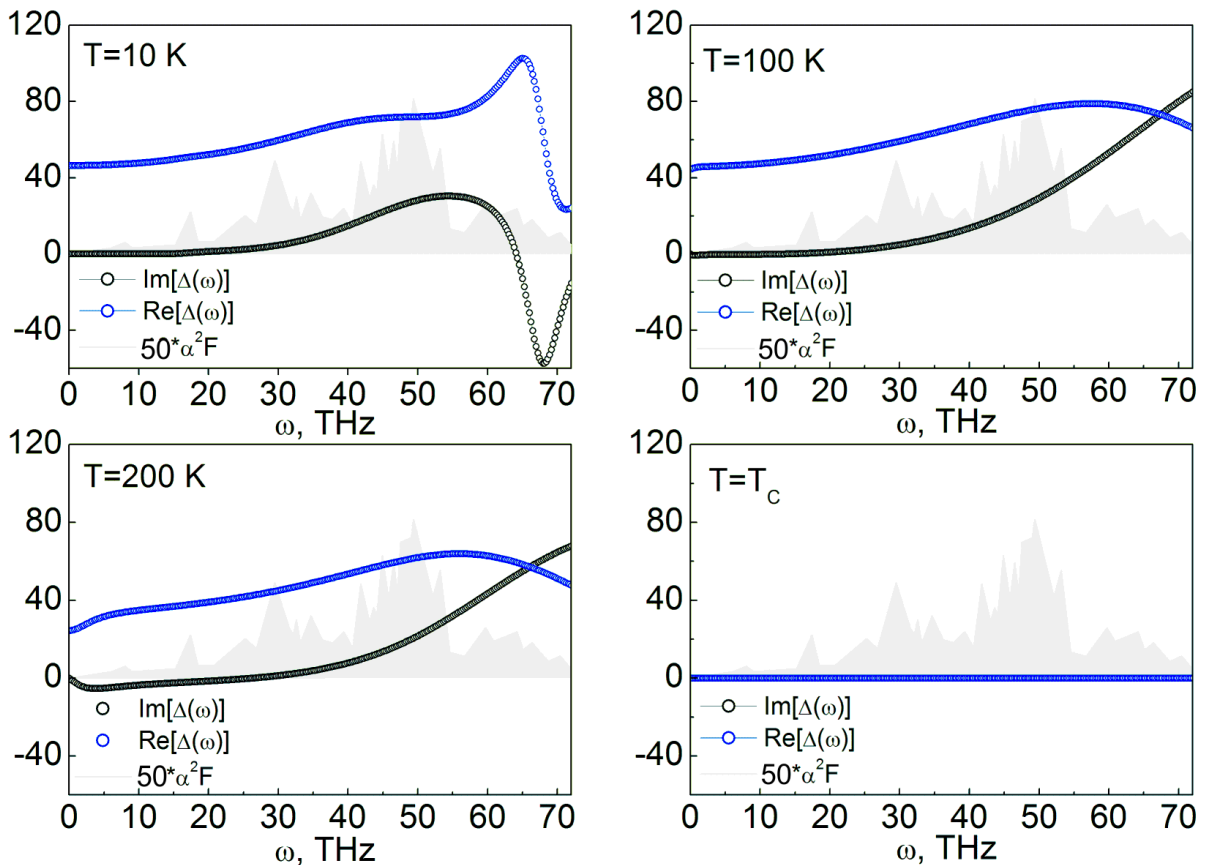


Fig. S3. The order parameter $\Delta(\omega)$ in meV for $P6/mmm$ -LaH₁₆ at 250 GPa on the real axis for the selected values of temperature ($\mu^* = 0.1$). In addition, the Eliashberg function (grey) was added as the background (multiplied by 50 for easier comparison).

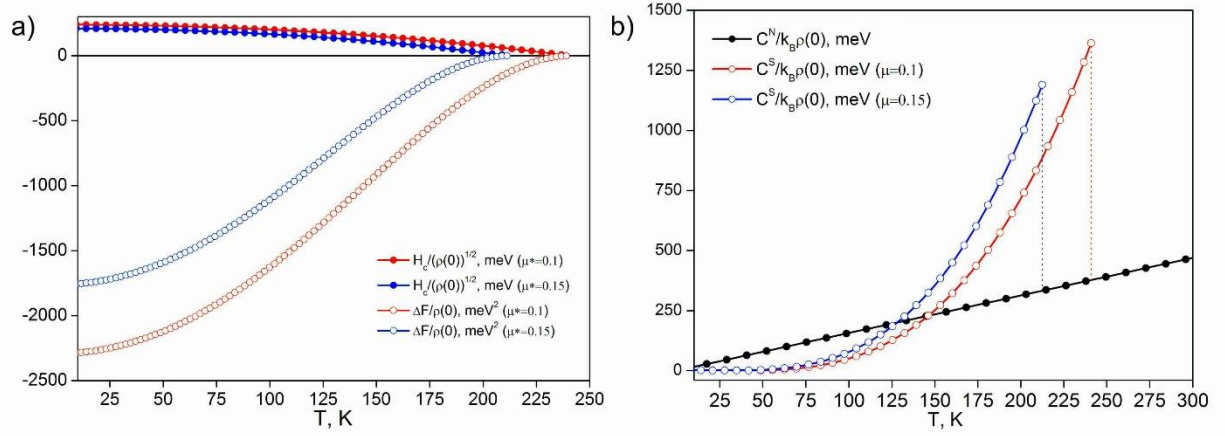


Fig. S4. a) The dependence of the thermodynamic critical field on the temperature (in meV, solid circles) and free energy difference between the superconducting state and the normal state as a function of the temperature (in meV 2 , open circles); b) The specific heat of the superconducting state (C_S) and the normal state (C_N) as a function of temperature. Here $\rho(0)$ is the density of states at the Fermi level.

Raman spectra

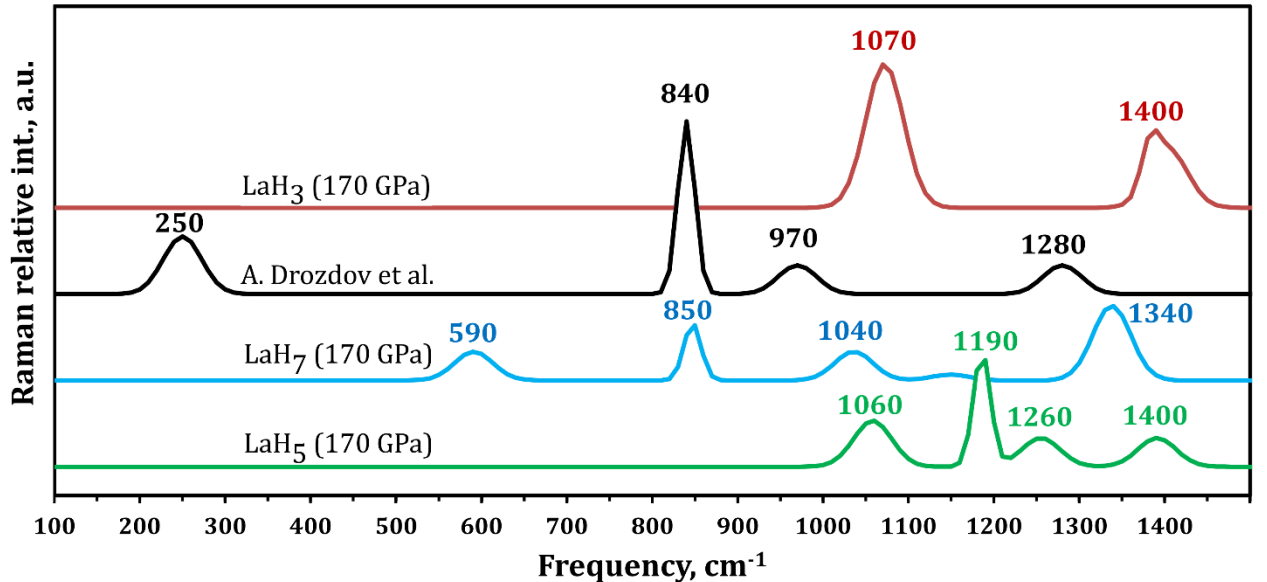


Fig. S5. Predicted Raman spectra of $Cmcm$ -LaH₃ (red), $Cmc2_1$ -LaH₇ (blue), $P\bar{1}$ -LaH₅ (green) and experimental results from Drozdov et al.⁹ (black) at 170 GPa.

Electronic and phonon properties of La-H phases

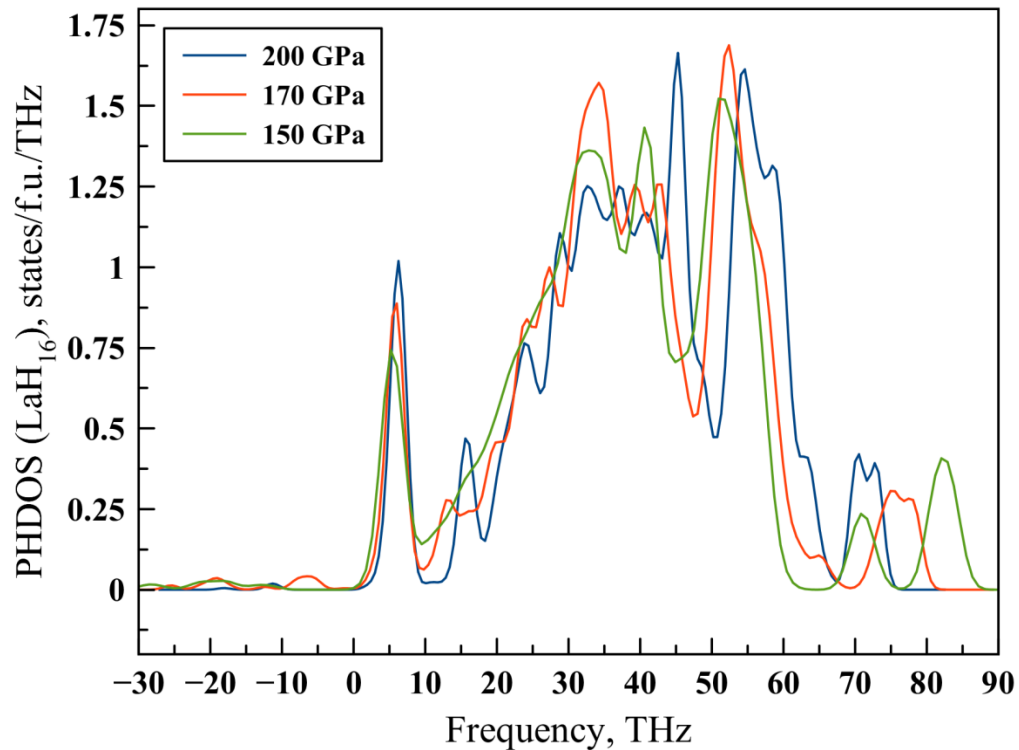


Fig. S6. Phonon density of states (DOS) of $P6/mmm$ -LaH₁₆ phase at 150, 170 and 200 GPa.

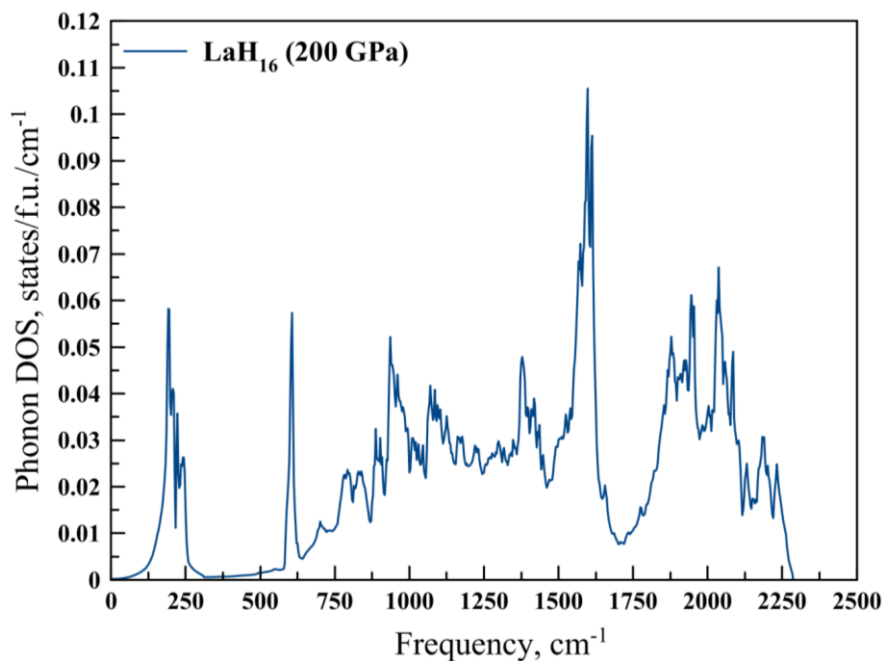


Fig. S7. Phonon DOS of $P6/mmm$ -LaH₁₆ at 200 GPa calculated in Quantum ESPRESSO.

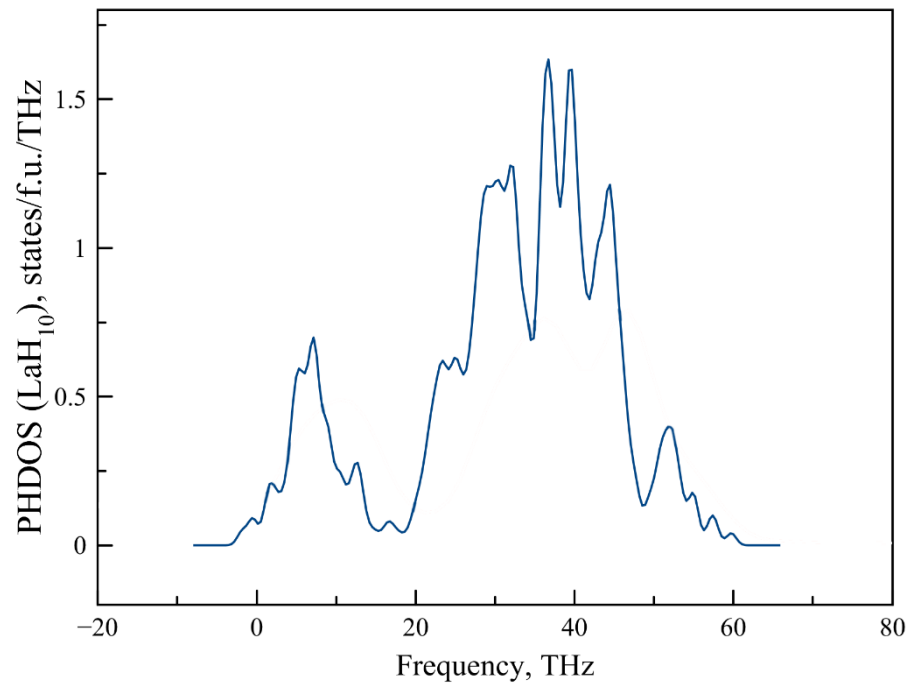


Fig. S8. Phonon density of states (smoothed) of $Fm\bar{3}m$ -LaH₁₀ at 150 GPa.

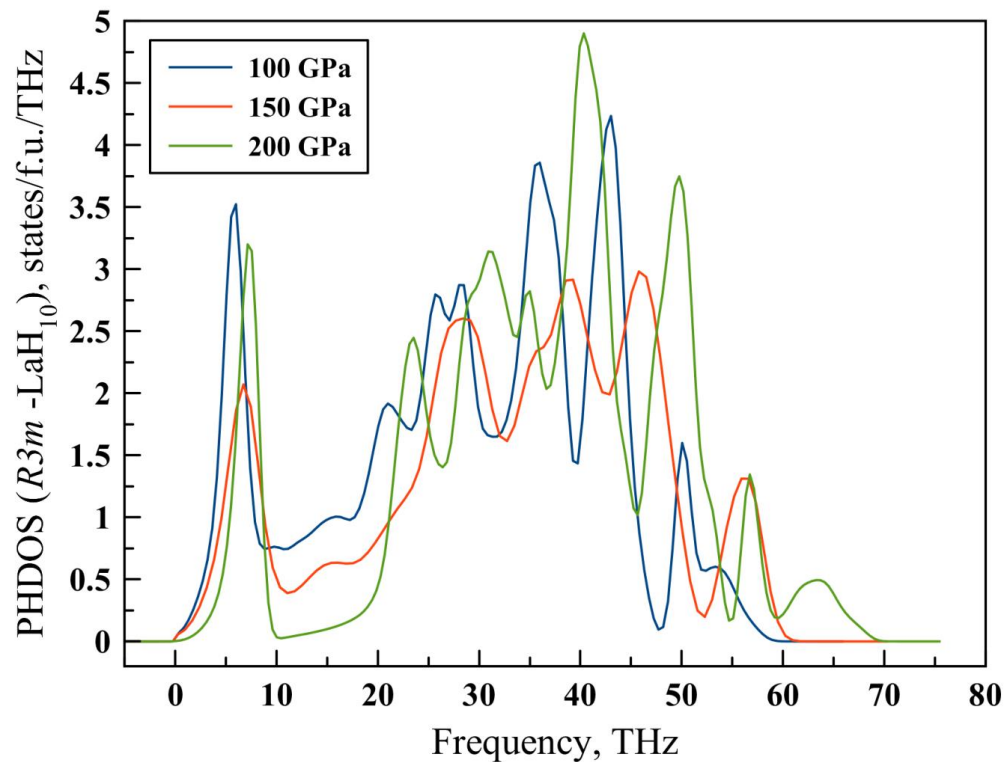


Fig. S9. Phonon density of states (smoothed) of $R\bar{3}m$ -LaH₁₀ at 100, 150 and 200 GPa.

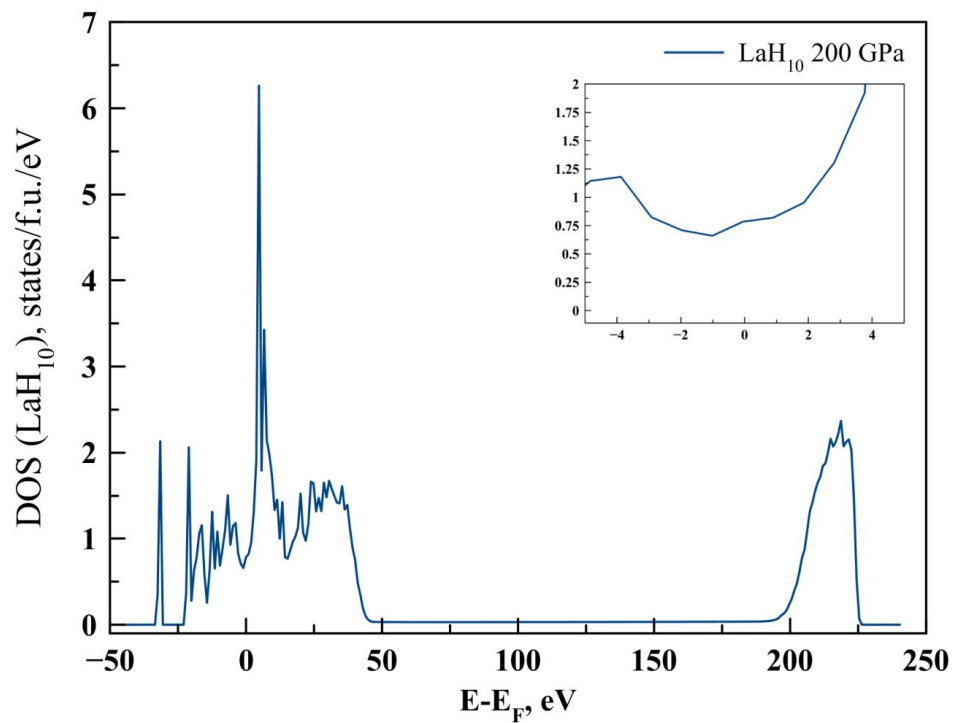


Fig. S10. Electronic density of states of $Fm\bar{3}m$ - LaH_{10} at 200 GPa.

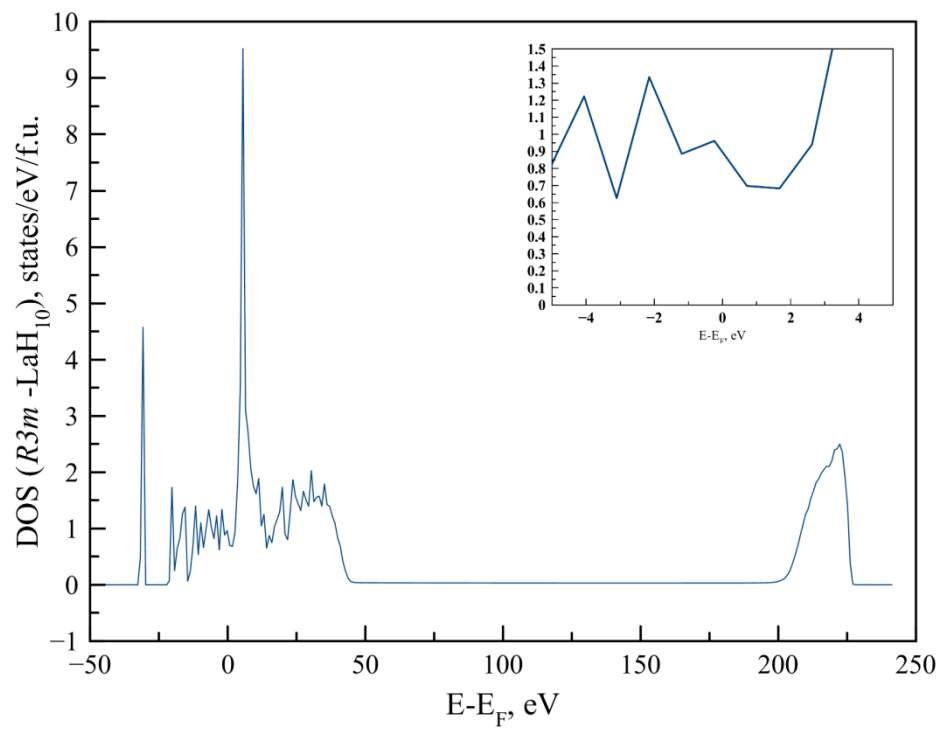


Fig. S11. Electronic density of states of $R\bar{3}m$ - LaH_{10} at 150 GPa.

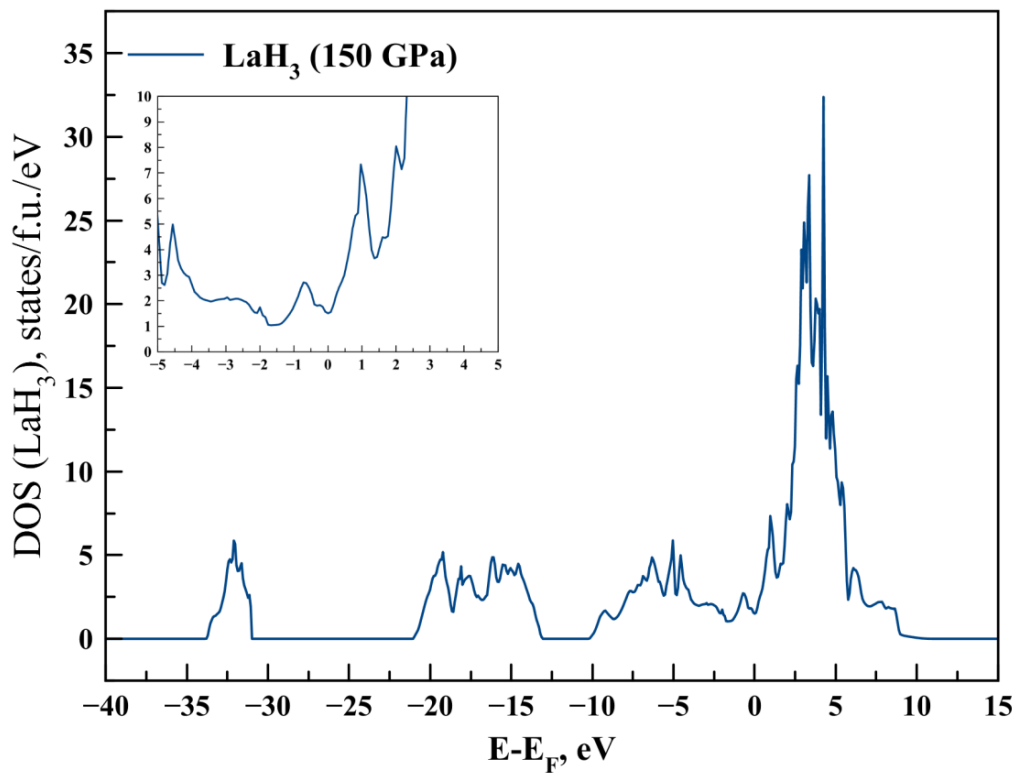


Fig. S12. Electronic density of states of $Cmcm$ - LaH_3 at 150 GPa.

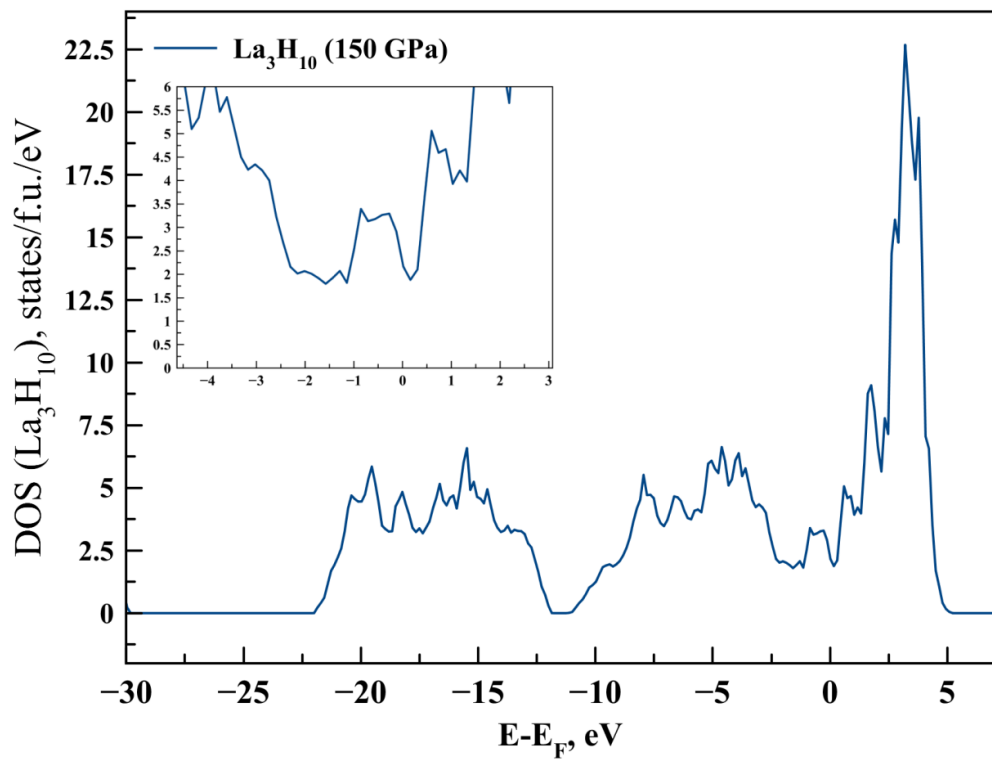


Fig. S13. Electronic density of states of $Cmmm$ - La_3H_{10} at 150 GPa.

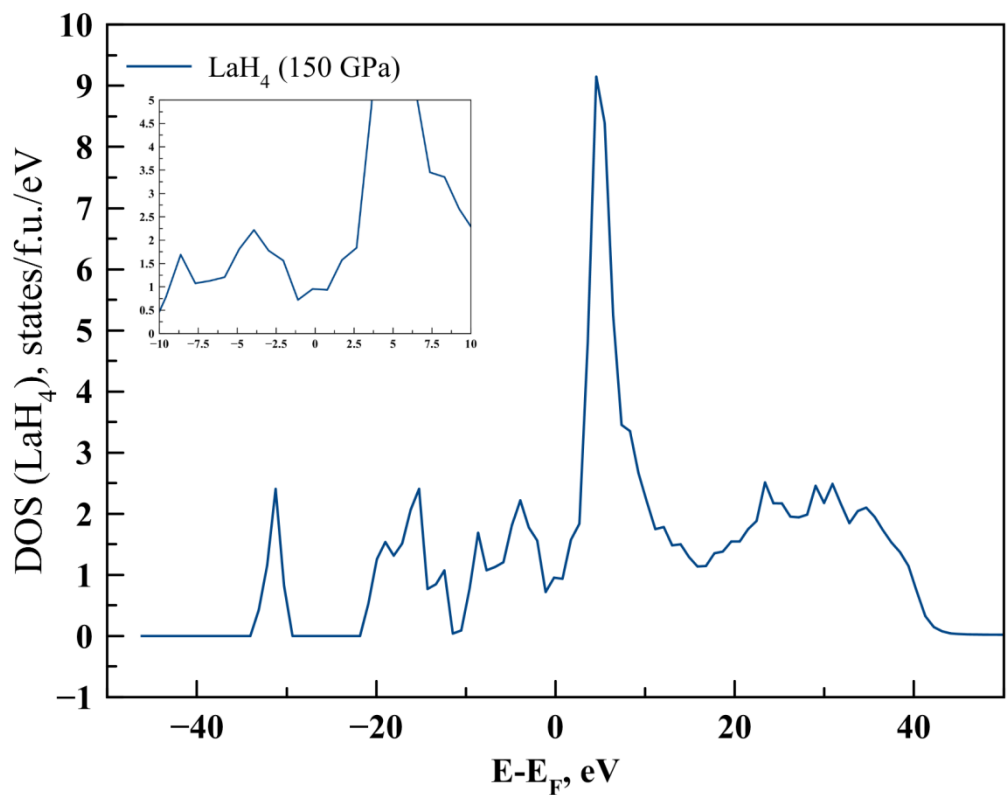


Fig. S14. Electronic density of states of $I4/mmm$ - LaH_4 at 150 GPa.

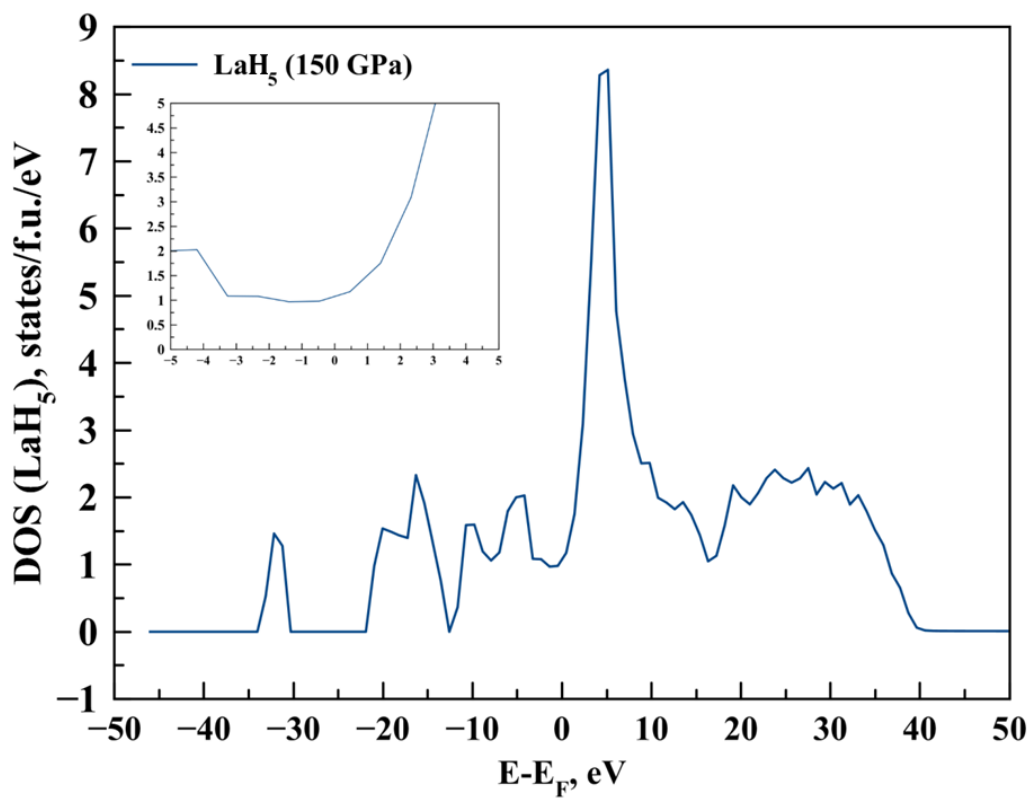


Fig. S15. Electronic density of states of $P\bar{1}$ - LaH_5 at 150 GPa.

Eliashberg spectral functions

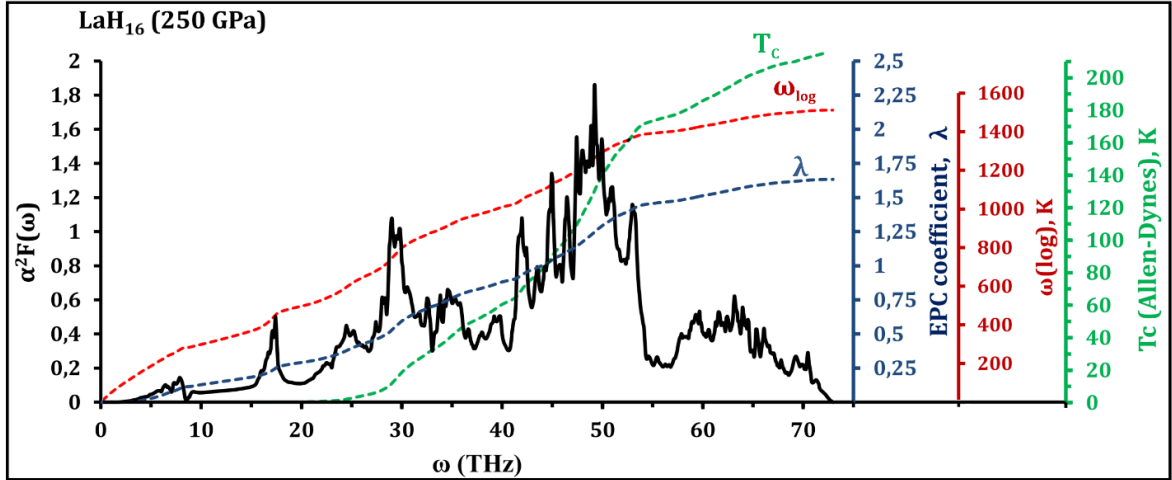


Fig. S16. Eliashberg function $\alpha^2 F(\omega)$ (black), ω_{\log} (red), EPC coefficient λ (blue), critical transition temperature T_c (green) of $P6/mmm$ - LaH_{16} at 250 GPa.

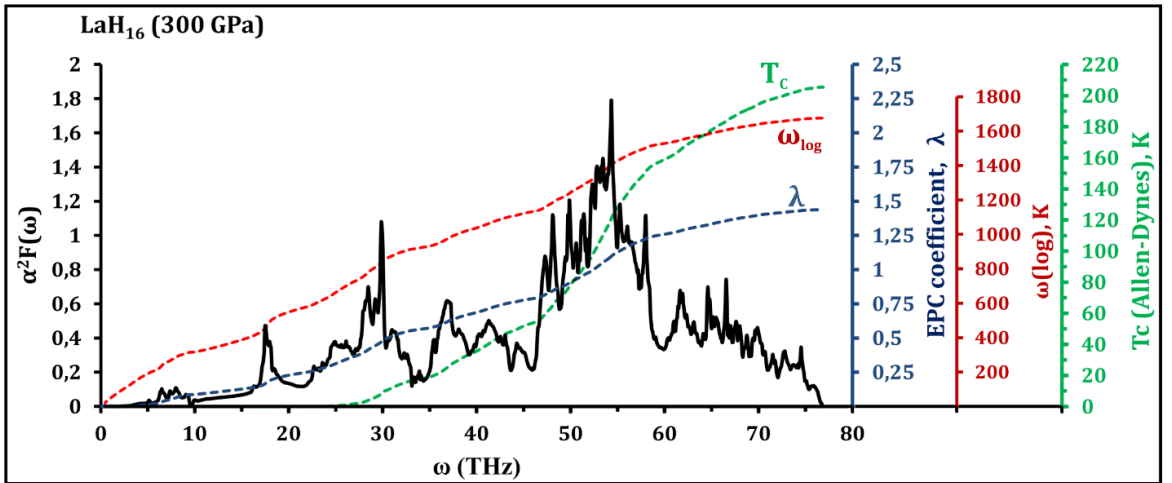


Fig. S17. Eliashberg function $\alpha^2 F(\omega)$ (black), ω_{\log} (red), EPC coefficient λ (blue), critical transition temperature T_c (green) of $P6/mmm$ - LaH_{16} at 300 GPa.

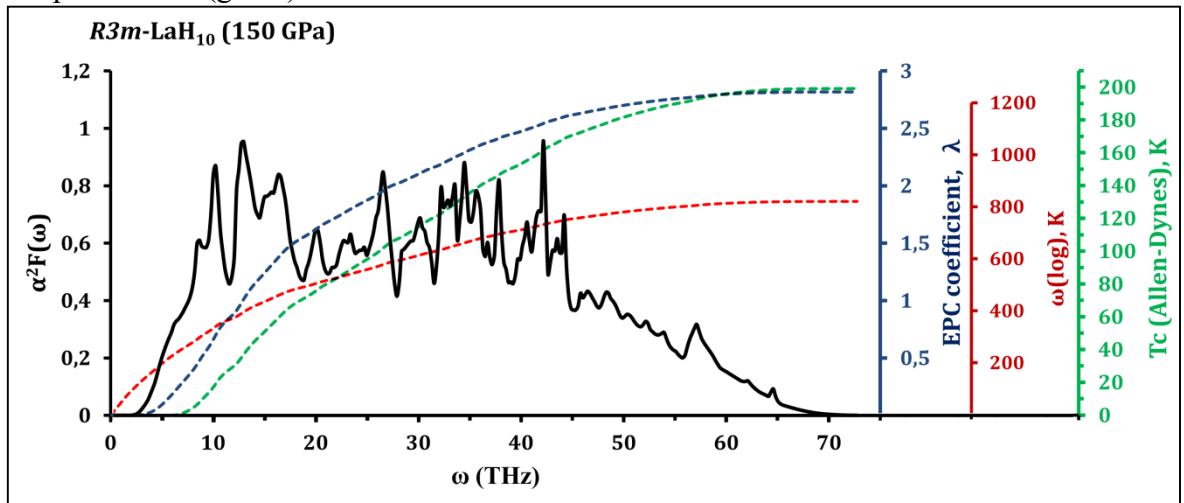


Fig. S18. Eliashberg function $\alpha^2 F(\omega)$ (black), ω_{\log} (red), EPC coefficient λ (blue), critical transition temperature T_c (green) of $R\bar{3}m$ - LaH_{10} at 150 GPa.

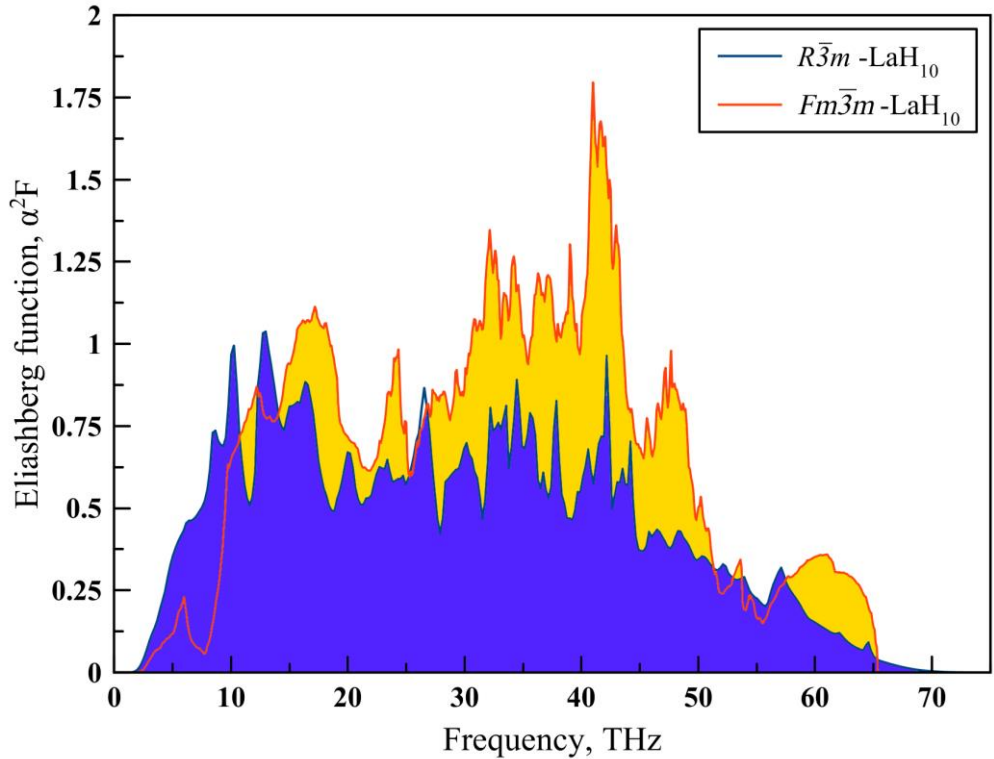


Fig. S19. Eliashberg functions $\alpha^2 F(\omega)$ of $R\bar{3}m$ -LaH₁₀ at 150 GPa (blue) and $Fm\bar{3}m$ -LaH₁₀ at 200 GPa (yellow).

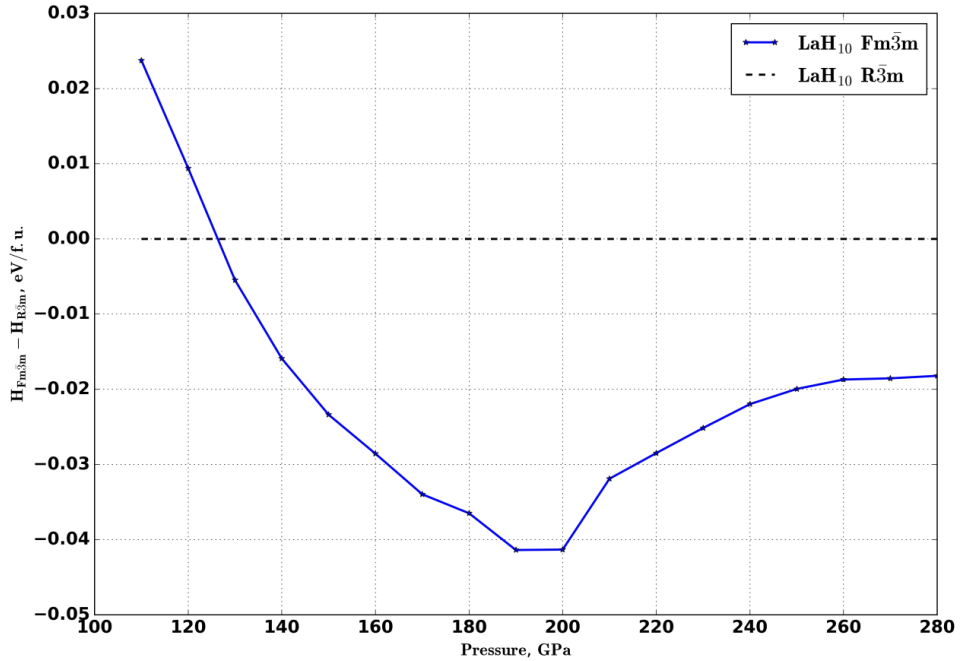


Fig. S20. Enthalpy difference between $Fm\bar{3}m$ -LaH₁₀ and $R\bar{3}m$ -LaH₁₀. Undoubtedly, the transition $Fm\bar{3}m \rightarrow R\bar{3}m$ plays an important role in the measured record superconductivity of LaH_{10+x}. Such structural transitions accompany superconductivity in H₃S ($C2/c \rightarrow R\bar{3}m \rightarrow Im\bar{3}m$),¹² in Nb₃Al, V₃Ga¹³ and in other well-known superconductors.

Matlab functions for T_c calculation using Allen's algorithm from Ref. 3

```

function Solve_Elisahberg(Ef, Tf, mu, filename)
% filename is the name of file with a2F function
N = 24;                                % dimension of the matrix  $K_{nm}$ 
mu = 0.1;                                % Coulomb pseudopotential,  $\mu^*$ 
T0 = 1;                                   % initial temperature
Tf = 300;                                 % final temperature
Th = 1;                                   % temperature step
h = 6.626070e-34;                         % Planck constant
k = 1.380e-23;                            % Boltzmann constant

t = T0:Th:Tf;                            % Temperature interval
%%% Read a2F function from file
a2F = load(filename);
wmax = max (a2F(:,1));                  % max frequency in Ry
wmin = min (a2F(:,1));                  % min frequency in Ry
l = length(a2F);                        % length of a2F
H = (wmax - wmin)/l;                    % Ry units

a2F(:,1) = a2F(:,1)* 13.6057 * 2.417e+14;    % convert Ry to Hz
%%% a2F(:,1) = a2F(:,1)* 1.0e+12;            % convert THz to Hz

T=1;
for j = 1:length(t)                      % Loop for temperature T=j
T=t(j);
    for y = 1:N+1                         % sum-function S(x), here we turn to the
        % function L(z,T) and calculate all the partial sums
        S1=0;
        for z=1:y
            S1 = S1+L(z,T,filename);
        end
        S(y)=S1;
    end

D=0;
for n=1:N+1                             % calculation of  $K_{mn}$  matrix in two cycles
    for m=1:N+1
        if n==m
            if m==1
                D = 2*(m-1)+1+L(0,T);
            else
                D=2*(m-1)+1+L(0,T)+2*S(m-1);
            end
        else
            D=0;
        end
        K(m, n)=L(m-n,T)+L(m+n-1,T)-2*mu-D;
    end
end
[A,B]=eig(K);                          %calculation of eigenvalues
B_max(j) = max(max(B));                % maximum eigenvalue
disp(t(j));
end
B_max = B_max';
plot([T0:Th:Tf],B_max(:,1),'r'); % graph crosses zero at the T = Tc
hold on

function [L] = L(R,T,filename)          % Function for electron-electron
interaction
% filename is the name of file with a2F function

```

```

N = 24;                                % dimension of the matrix K_nm
h = 6.626070e-34;                      % Planck constant
k = 1.380e-23;                          % Boltzmann constant

%%%Read a2F function from file
a2F = load(filename);
l = length(a2F);                        % length of a2F
a2F(:,1) = a2F(:,1)* 13.6057 * 2.417e+14;    % convert Ry to Hz
%%%a2F(:,1) = a2F(:,1)* 1.0e+12;            % convert THz to Hz

Int = 0;
for xx=1:l-1
    Int = Int + (a2F(xx+1,1)-a2F(xx,1))*2*a2F(xx,2)*(h^2)*...
        a2F(xx,1)/((h*a2F(xx,1))^2 + (6.283*(R)*k*T)^2);
end
L=Int;

% It should be noted that the lines a2F = load(filename) in L.m function and
% in the main script must be changed simultaneously.

```

References

- (1) Eliashberg, G. M. Interactions between Electrons and Lattice Vibrations in a Superconductor. *JETP* **1959**, *11* (3), 696–702.
- (2) Bergmann, G.; Rainer, D. The Sensitivity of the Transition Temperature to Changes in $A2F(\omega)$. *Z. Für Phys.* **1973**, *263* (1), 59–68.
- (3) Allen, P. B.; Dynes, R. C. A Computer Program for Numerical Solution of the Eliashberg Equation to Find T_c . *Tech. Rep. 7 TCM41974* **1974**.
- (4) Szczęśniak, R. The Numerical Solution of the Imaginary-Axis Eliashberg Equations. *Acta Phys. Pol. A* **2006**, *109* (2), 179–186.
- (5) Szczęśniak, R. The Selected Thermodynamic Properties of the Strong-Coupled Superconductors in the van Hove Scenario. *Solid State Commun.* **2006**, *138* (7), 347–352.
- (6) Durajski, A. P.; Szczęśniak, D.; Szczęśniak, R. Study of the Superconducting Phase in Silicene under Biaxial Tensile Strain. *Solid State Commun.* **2014**, *200*, 17–21.
- (7) Beach, K. S. D.; Gooding, R. J.; Marsiglio, F. Reliable Pad'e Analytical Continuation Method Based on a High-Accuracy Symbolic Computation Algorithm. *Phys. Rev. B* **2000**, *61* (8), 5147–5157.
- (8) Bardeen, J.; Cooper, L. N.; Schrieffer, J. R. Theory of Superconductivity. *Phys. Rev.* **1957**, *108* (5), 1175–1204.
- (9) Drozdov, A. P.; Minkov, V. S.; Besedin, S. P.; Kong, P. P.; Kuzovnikov, M. A.; Knyazev, D. A.; Eremets, M. I. Superconductivity at 215 K in Lanthanum Hydride at High Pressures. *ArXiv180807039 Cond-Mat* **2018**.
- (10) Somayazulu, M.; Ahart, M.; Mishra, A. K.; Geballe, Z. M.; Baldini, M.; Meng, Y.; Struzhkin, V. V.; Hemley, R. J. Evidence for Superconductivity above 260 K in Lanthanum Superhydride at Megabar Pressures. *ArXiv180807695 Cond-Mat* **2018**.
- (11) Liu, H.; Naumov, I. I.; Hoffmann, R.; Ashcroft, N. W.; Hemley, R. J. Potential High- T_c Superconducting Lanthanum and Yttrium Hydrides at High Pressure. *Proc. Natl. Acad. Sci.* **2017**, *114*, 6990–6995.
- (12) Kruglov, I.; Akashi, R.; Yoshikawa, S.; Oganov, A. R.; Esfahani, M. M. D. Refined Phase Diagram of the H-S System with High- T_c Superconductivity. *Phys. Rev. B* **2017**, *96* (22), 220101.
- (13) Viswanathan, R. Martensitic Transformations in V_3Ga and Nb_3Al . *Mater. Res. Bull.* **1974**, *9* (3), 277–281.